

Article

Seepage Velocity: Large Scale Mapping and the Evaluation of Two Different Aquifer Conditions (Silty Clayey and Sandy)

Qais Al-Madhloom ^{1,2}, Nadhir Al-Ansari ^{1,*}, Bashar Abid Hamza ², Jan Laue ¹ and Hussain Musa Hussain ³

¹ Department of Civil, Environmental and Natural Resources Engineering, Lulea University of Technology, 97187 Luleå, Sweden; qais.alsaady@gmail.com or qais.al-madhloom@ltu.se (Q.A.-M.); jan.laue@ltu.se (J.L.)

² Faculty of Engineering/Al-Musayab, University of Babylon, Musayyib 51006, Iraq; basharabid74@gmail.com

³ Remote Sensing Center, University of Kufa, Kufa 540011, Iraq; hussainm.alshimmary@uokufa.edu.iq

* Correspondence: nadhir.alansari@ltu.se; Tel.: +46-7253-907-67

Received: 27 July 2020; Accepted: 14 August 2020; Published: 18 August 2020



Abstract: Seepage velocity is a very important criterion in infrastructure construction. The planning of numerous large infrastructure projects requires the mapping of seepage velocity at a large scale. To date, however, no reliable approach exists to determine seepage velocity at such a scale. This paper presents a tool within ArcMap/Geographic Information System (GIS) software that can be used to map the seepage velocity at a large scale. The resultant maps include both direction and magnitude mapping of the seepage velocity. To verify the GIS tool, this study considered two types of aquifer conditions in two regions in Iraq: silty clayey (Babylon province) and sandy (Dibdibba in Karbala province). The results indicate that, for Babylon province, the groundwater flows from the northwest to southeast with a seepage velocity no more than 0.19 m/d; for the Dibdibba region, the groundwater flows from the west to the east with a seepage velocity not exceeding 0.27 m/d. The effectiveness of the presented tool in depicting the seepage velocity was thus demonstrated. The accuracy of the resultant maps depends on the resolution of the four essential maps (groundwater elevation head, effective porosity, saturated thickness, and transmissivity) and locations of wells that are used to collect the data.

Keywords: darcy velocity large scale mapping; seepage velocity large scale mapping; average linear velocity large scale mapping; ArcMap/GIS software; groundwater tools; darcy velocity tool; thermal advection losses; heat transfer with porous media; mass transfer porous media; contaminants transfer within soil

1. Introduction

Groundwater represents a promising solution for one of the most significant problems facing humanity in recent decades. Amongst many significant complex problems, such as resource depletion, poverty, ecosystem service deterioration, pollution, biodiversity loss, and climate change and global warming [1–4], the shortage of water represents the greatest threat because it is directly related to human wellbeing [5,6]. According to the World Resources Institute (WRI), numerous countries have experienced serious problems regarding quality and quantity of water resources, and many more countries will face these problems in the future [7,8]. The Tigris and Euphrates river basin (spanning parts of Turkey, Syria, Iraq, and Iran) lost about 144 cubic kilometers of fresh water between 2003 and 2009. This loss is roughly equivalent to the volume of the Dead Sea [9]. The total loss of all water resources in the basin between 2003 and 2010 has been estimated to be a depth of about 200 mm [10], resulting in drought, and affecting the marshes of south Iraq [11–14].

Groundwater is the most suitable solution to the problem of water shortages [15] because it is more reliable and predictable compared to surface water under current conditions [16,17]. During 2015, groundwater represented the major source of fresh water for approximately 2 billion people globally [17].

Although groundwater is more reliable than surface water, it can also be depleted due to anthropogenic activities (mismanagement) and global climate change [18,19]. Most aquifers around the world are overstressed and subject to depletion because the water withdrawn surpasses the recharged volume [17,20]. About 60 percent (equivalent to 90 cubic kilometers) of the loss of the total water resources in the Tigris and Euphrates river basin during the 2003–2010 period was attributed to the pumping of groundwater from underground reservoirs [9]. The depletion in groundwater for the basin was equivalent to a fall in the water level of about 140 mm during the same period (2003–2010) [10].

A large number of applications in civil engineering relate to groundwater flow, such as slope stability [21–23]; surface/subsurface soil erosion and sediment transport [24–26]; dam safety, including piping under and through dams [27–32]; groundwater contamination [33–36]; stability of artificially freezing ground [37,38]; sustainable management of water resources [39–42]; interaction between groundwater and surface water [43,44]; and karst collapse pillars [45–47].

Two additional important sustainable applications related to groundwater flow are geothermal systems and underground thermal energy storage (UTES) systems [48–59]. These systems were first used due to the oil crisis of the 1970s to identify alternative sources of energy [60,61], and have subsequently been proven to be successful in solving various challenges. Global warming represents an additional challenge [62,63]. As a result of their demonstrated feasibility, these systems are now widely spread across Europe and North America [64–66]. However, they are still not well known in Middle Eastern countries, despite the potential advantages that the systems could offer in this region [67–72].

In practice, all of the previously mentioned applications of groundwater engineering are related to groundwater seepage. Due to the hydraulic conditions of global groundwater, it is seldom under static conditions [73,74], and flows from high to low hydraulic head regions [75,76]. The flow of groundwater is subject to Darcy's law [75,76]. Darcy's law states that Darcy flux, which can misleadingly be called Darcy velocity, is proportional to hydraulic gradient [77]. The constant of the proportion is the hydraulic conductivity of the porous medium (aquifer). Darcy flux is also known as the specific discharge or the volumetric flow rate per unit area of the aquifer. The velocity of the groundwater can be more accurately represented by the seepage velocity, which is also called average linear velocity or average pore velocity through a porous medium. Seepage velocity represents the average velocity of flowing groundwater within pores of a porous medium, and is derived by dividing Darcy flux by the effective porosity [73,75,76,78].

In the study area considered for this article (Babylon and Karbala regions in the middle of Iraq), it is expected that Aquifer Thermal Energy Storage (ATES) systems will be used in the future rather than conventional Heating Ventilation Air Conditioning systems. This expectation is consistent with the Middle East and North Africa (MENA) orientation to expand the use of renewable energy instead of fossil fuel [79–83]. Feasibility studies of ATES systems should be conducted prior to installation. One approach involves numerical simulation of ATES systems to identify potential problems and potential solutions [84,85]. Seepage velocity is a significant variable in these simulations, in addition to representing the simulation's boundary conditions. Therefore, it is important to determine the seepage velocity within a given study area [86,87].

Numerous software packages are used to simulate the movement of groundwater in the soil and aquifers, including Groundwater Modelling System (GMS) [88–91]; Visual MODFLOW Flex [92–95]; and ModelMuse [96–99]. Most of these packages require inputting the seepage velocity as the boundary or initial conditions to conduct the simulation. In this study, Visual MODFLOW Flex was used to analyze the utilization of aquifers in the study area (Babylon and Dibdibba within Karbala) as thermal energy storage systems. The MODFLOW software was used to analyze operations under different scenarios, and to explore the consequences of using these aquifers as thermal storage.

Different features and properties of the ATEs system must be studied prior to its implementation such as storage efficiency, Coefficient of Performance (COP) for the planned heating/cooling system, and the effect of the system on the groundwater table and potential soil settlement. Therefore, mapping of the seepage velocity at a large scale is required as an input to the analysis software. Furthermore, most groundwater simulation packages allow the import of Geographic Information Systems (GIS) files, which makes seepage velocity maps produced with a GIS extension useful for simulating groundwater systems [100–102].

Another benefit of mapping seepage velocity at a large scale is the innovative use of the site selection of the UTES system [71,103]. Seepage velocity maps are used in the determination of the optimal location to install the UTES systems. These maps are a significant input to the process because determining the optimal location requires minimizing the advection losses, i.e., minimizing seepage velocity [71,103].

Despite the importance of seepage velocity in engineering applications, such as heat transfer [34,37,51] and aquifer pollution [104–106], few published papers exist that consider the mapping of seepage velocity (direction and magnitude) at a large scale. A large number of studies have been conducted to simulate seepage velocity at a small scale [52,107,108], but no previous studies (with the exception of those conducted by the authors of the current paper) have investigated seepage velocity on a large scale. Therefore, this study presents a straightforward approach to mapping seepage velocity at a large scale. In addition, the produced seepage velocity maps can be used in other disciplines, e.g., optimizing the water resource management of the study area and preventing deterioration of Iraq's water resources [10], in addition to the engineering applications noted previously. Thus, the problem addressed by this study can be formulated as the following two questions: "How can seepage velocity maps (direction and magnitude) be produced?", and "What tools are required to produce these maps?". To provide a better understanding of the considered tools and seepage velocity, a third research question can be added: "What are the differences in the seepage velocity between two cases of aquifers: silty clayey and sandy?".

It should be noted that the use of ATEs systems is important for all countries trying to reduce their energy consumption. To apply a suitable method or techniques, the seepage velocity must be known within the area concerned. In addition, knowledge of seepage velocity also helps in the identification of a suitable site to install these systems. This paper advances a tool within ArcMap/GIS software that can be used to determine the seepage velocity (magnitude and direction) for large-scale mapping. The results can subsequently be used as an input in the simulation of ATEs systems using MODFLOW Flex, and to find the optimal location for the installation of ATEs systems using the site selection approach [71,103]. To illustrate the use of the presented tool and determine the differences in seepage velocity between two aquifer types (silty clay and sandy), two regions within Iraq were considered: Babylon and part of Dibdibba basin within Karbala.

2. Study Area

The study area comprises two regions: Babylon province and a portion of the Dibdibba basin within Karbala province (Figure 1). A description of each region is provided below.

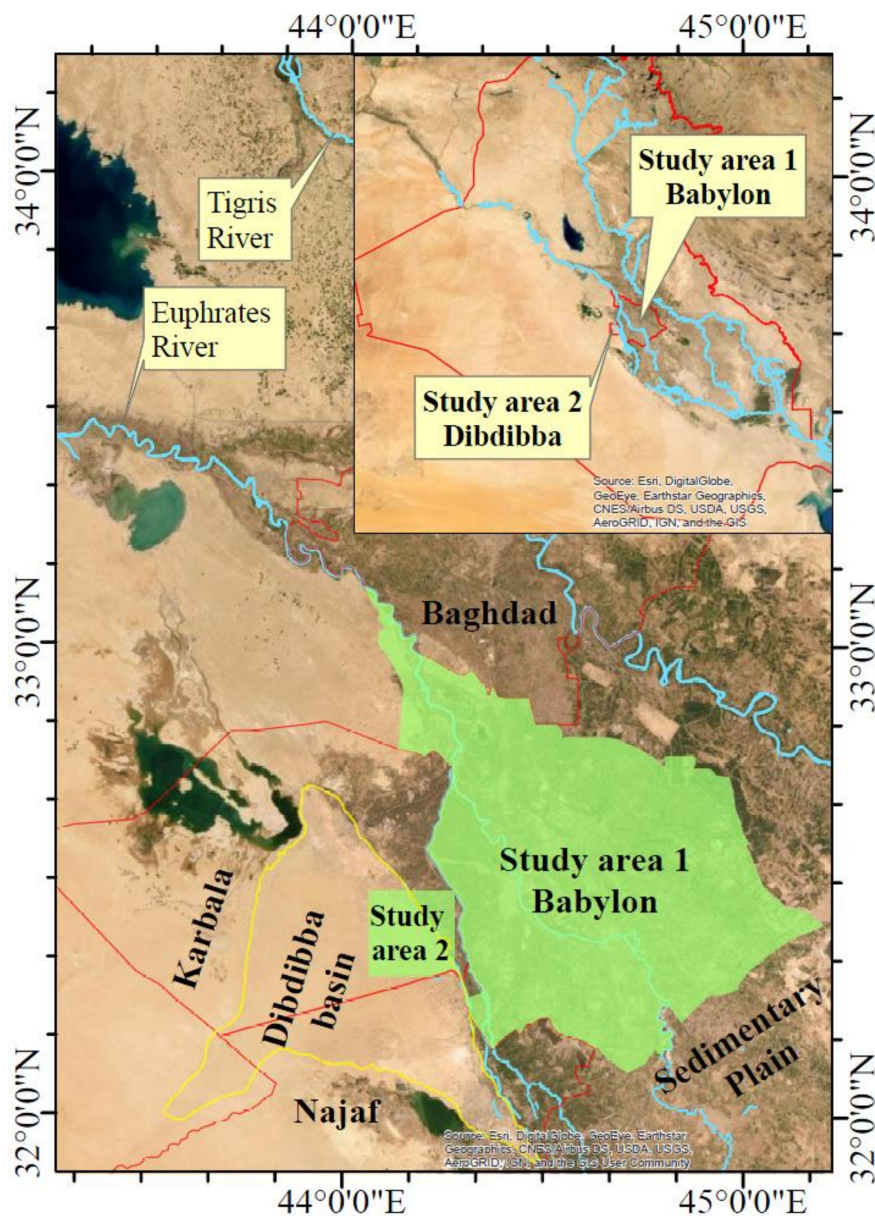


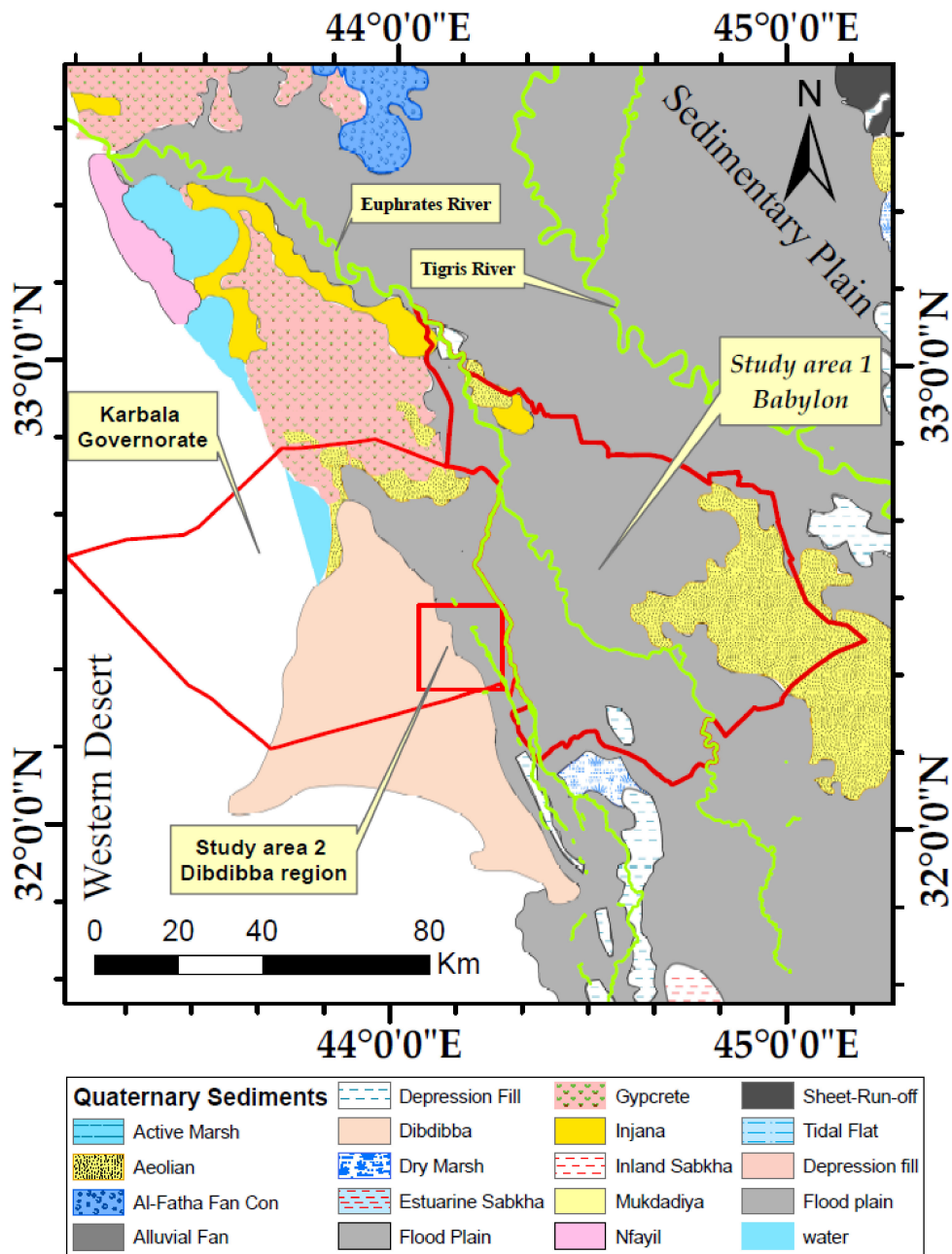
Figure 1. Study area (Babylon and Dibdibba aquifers within Iraq) projected on satellite images [109].

2.1. Babylon

Babylon province is located in the middle of Iraq, about 100 km south the capital Baghdad (Figure 1). Its area is about 5135 km², and has a population of about 2 million. It is bounded by the longitudes 44°2'42" E and 45°12'1" E and the latitudes 32°5'54" N and 33°7'35" N; see Figures 1 and 2a. It is part of the sedimentary plain (Mesopotamia zone) of Iraq (Figure 2a). The ground surface has a gentle slope from the northwest toward the southeast. The elevation of the ground in the north is about 72 m.a.s.l. (meters above sea level), and is about 11 m.a.s.l. in the southern areas; see Figure 2b. The slope of the ground surface ranges from 0% to 16.5%. About 96% of the ground surface in the province has a slope less than 2% (20 m/km), and 3.8% has a slope ranging from 2% to 4% (40 m/km).

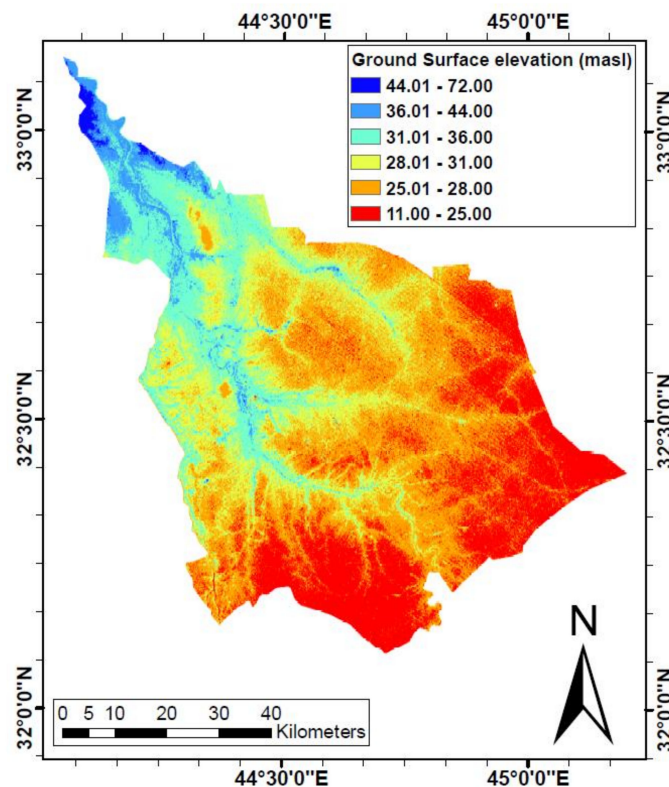
The province is mainly covered by Quaternary sediment [110]; see Figure 2. Most of these Quaternary sediments are eroded and transported by the Euphrates and Tigris Rivers from the northern parts of their basins and along their courses. The Euphrates River flows through Babylon province from the northwest toward the southeast. There are mainly two types of Quaternary geomorphological units

exposed in this region: the prevail flood plain and Aeolian (southeast) landforms. Both of these belong to the Holocene epoch, the most recent series within the Quaternary Period [110,111]; see Figure 2a.



(a)

Figure 2. Cont.



(b)

Figure 2. Babylon study area, (a) geomorphology of Babylon study area, (b) ground surface elevation (m.a.s.l.) map; a modified after [112].

Stratigraphically, the Quaternary sediments in this region can be further divided into layers based on the geological epoch (period). Ranked from the bottom to the top, these layers are:

- Mesopotamia fluvial basin sediments: these are fluvial sediments belonging to the Pleistocene epoch and comprising inner bedding varying from sandy gravel to silty clay. Sand prevails in this layer followed by silt. Its thickness ranges from 58 to 174 m [111];
- river terraces: these are well developed along the cliffs bordering the Euphrates flood plain in the vicinity of Iskandariyah. They belong to the Pleistocene epoch. They comprise inter-bedding ranging from sandy gravel to sand; however, local laminated horizons of silty clay are also found in some places. Their thickness reaches 6 m in the vicinity of Iskandariyah [111];
- flood plain sediments: Babylon province can be represented by a vast fertile flood plain comprising the Euphrates (primary) and Tigris (secondary) rivers. These sediments belong to the Holocene epoch. They consist predominantly of silty clay, but loamy sand and sandy loam are also recorded frequently. Their thickness ranges from 15 to 20 m [111];
- Aeolian sediments: these are situated in the southeastern parts of the province. It is believed that these sediments belong to the late Holocene epoch. The sediments essentially comprise fine sand, silt, and clay. The main sources of these sediments are the flood plain sediments of the Euphrates and Tigris rivers. Its thickness reaches 5 m [111–113].

The Quaternary sediments are underlain by the Pre-Quaternary sediments, which are classified into a number of easily distinguishable formations. The Pre-Quaternary formations comprise Dibdibba, Mahmudiya, and Bai Hasan formations. All of these are fluvial sedimentary rocks [111].

Considering the geo-hydrological conditions, there are two aquifers systems in this region. The first is present within the Quaternary system/formations in the region. The upper fine particle

layers of the sediments represent the aquitards, while the deeper coarse particle layers of the sediments represent the aquifers. The second aquifer system is available within the Pre-Quaternary systems. Pre-Quaternary formations, such as Bai Hassan and Mukdadiya, are also in a hydraulic continuity with the first system of aquifers, thus, the Quaternary formations produce the second aquifer system (Pre-Quaternary system) [114,115]. The groundwater table within the study area is very shallow; it is less than 9 m below the ground surface (m.b.g.s.) [115]. Furthermore, some regions have a groundwater table of less than 2 m depth [72]; see Figure 3. For the Babylon region, the elevation of the water table is not characterized by sensitive variation. This is mainly because of the low dependence of the region on groundwater due to the presence of the surface water. Other reasons include regional characteristics such as its hydrology, topography, and stratigraphy, and the presence of barrages and regulators that control the surface water elevation and thus control the seepage from rivers and canals that are not lined.

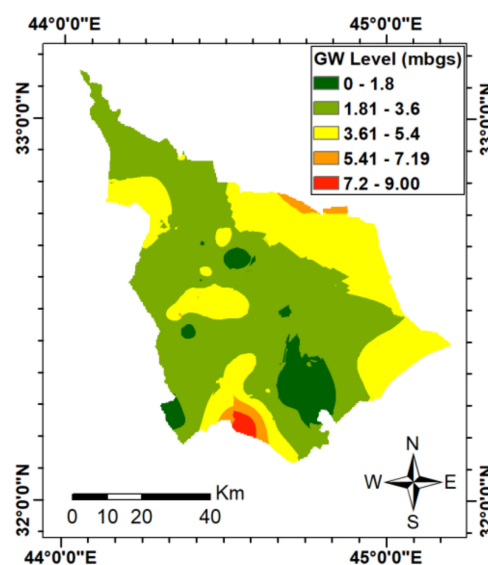


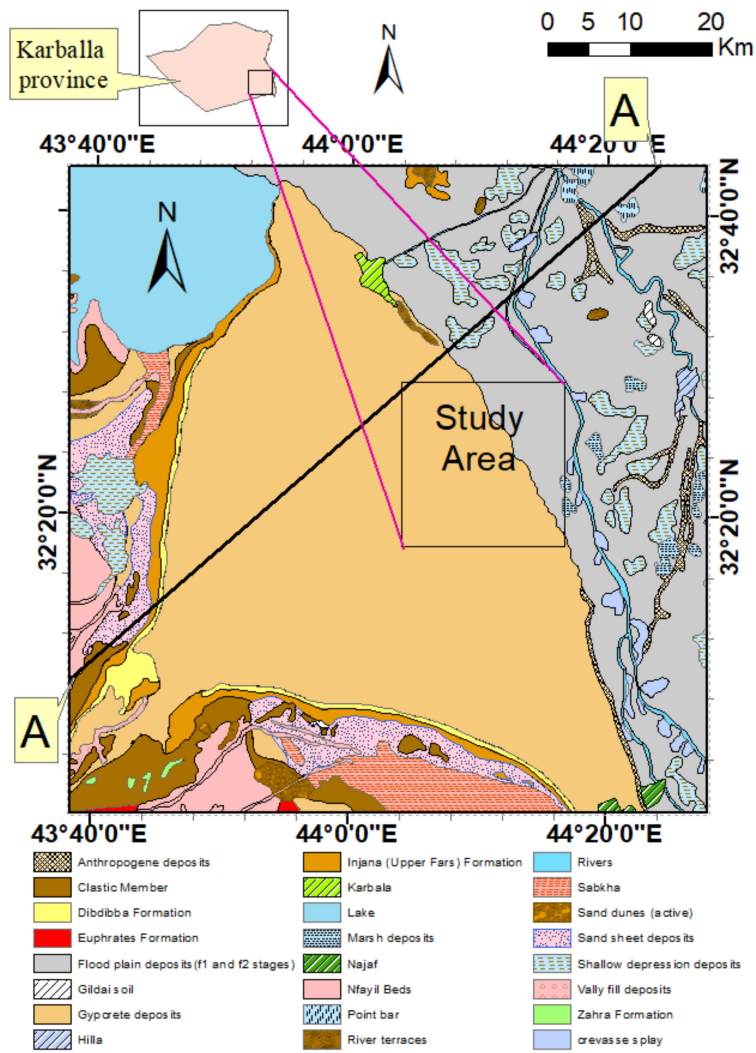
Figure 3. Groundwater table depth within Babylon study area (meters below the ground surface, m.b.g.s.) [71].

The climate of Babylon province is arid to semi-arid. The annual average precipitation is between 100 and 150 mm/year. The mean annual temperature is about 24 °C. In summer, the temperature can exceed 50 °C, can drop below 0 °C at nights in winter. The mean annual evaporation ranges from 3.4 to 3.5 m/year [72,115].

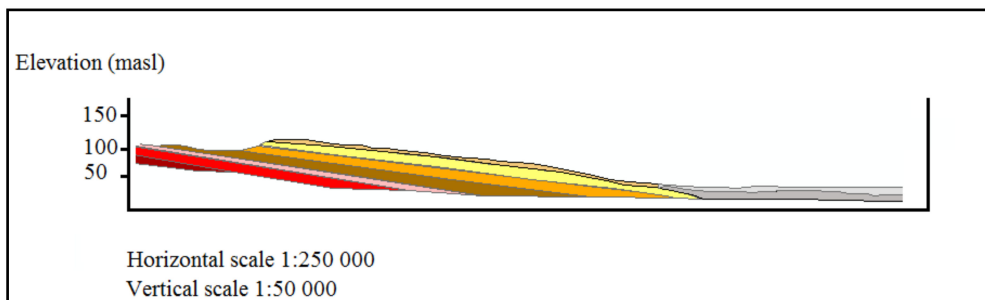
2.2. Dibdibba Basin

The second region in the study area is a portion of the Dibdibba basin, which is located in the plateau of the Karbala-Najaf region within the Western Desert of Iraq [116]; see Figure 4a. The overall Dibdibba basin is cone-shaped and encompasses an area of about 2700 km² [117]. The studied portion is situated in the southeastern area of Karbala province (Figures 1 and 2a). It can be represented by a square region with sides of 20 km length and an area of 400 km². It is bounded by the longitudes 44°3'55" E and 44°16'35" E and the latitudes 32°17'58" N and 32°28'52" N; see Figures 1, 2a and 4c.

The ground surface in the considered region has a slope from the west (more accurately, southwest) toward the east (more accurately, northeast). The elevation in the southwestern corner is about 83 m.a.s.l., and is about 25 m.a.s.l. at the east edge of the region; see Figure 4c. The slope of the ground surface ranges from 0% to 9.4% (94 m/km). About 80% of the ground surface in the region has a slope less than 1.9% (19 m/km), and 19% has a slope ranging from 1.9% to 3.8% (38 m/km).

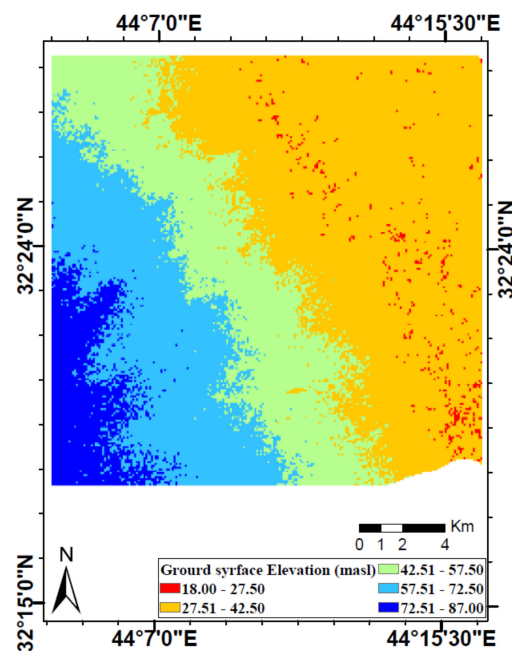


(a)



(b)

Figure 4. Cont.



(c)

Figure 4. Dibdibba study area, (a) geomography; (b) section A-A in Figure 4a above, (c) ground surface elevation (m.a.s.l.); a and b modified after [117].

The soil types in this region can be classified into two types: Gypcrete and fluvial silty clayey loam soil (Figure 4a,b). The Gypcrete type covers the western and southwestern parts of the region, while the silty clayey loam soil covers the eastern and the northeastern parts of the region. The western part is a portion of Iraq's Western Desert, and the eastern part is a portion of the Mesopotamia Plain. The eastern part is similar to the Babylon region in stratigraphy, and the western part is similar to the Western Desert of Iraq; see Figure 4b. Gypcrete, which covers the western portion of the Dibdibba study area, is a soil type from Quaternary deposits. Gypcrete can be defined as "a gypsiferous ($\text{CaSO}_4 \cdot 2\text{H}_2\text{O}$) soil profile developed in arid regions. Gypcrettes are formed by the precipitation of CaSO_4 from saline waters drawn to the surface by capillary action" [118]. This layer is covered by a thin veneer of sand sheets and scattered pebbles. The percentage of SO_4 is extremely variable. The thickness of the Gypcrete layer ranges from 0.5 to 2.0 m [116]. The Gypcrete layer is underlain by the Dibdibba formation, which represents the body of the aquifer, and belongs to the Pliocene–Pleistocene epoch; see Figure 4b. It mainly consists of poorly sorted sand and sandstone, and gravel of igneous rocks. Its thickness ranges from 3 to 15.5 m [111,116]. The Dibdibba formation is underlain by the Injana (Upper Miocene) formation, which is in turn underlain by the Nfayil (Middle Miocene) formation, then the Euphrates (Early Miocene) formation; see Figure 4b [119,120]. The Injana formation represents an aquitard bed for the Dibdibba formation, such that the groundwater flows within the direction of the dip of both the Dibdibba and Injana formations [111].

The depth of the water table in this region ranges from 48 m.b.g.s. in the southwestern corner to about 2 m.b.g.s. in the northeast corner (Figure 5). The shallow water table is one of the three reasons for the development of Gypcrete soil in the region. The other two reasons are groundwater composition and the arid climate [121]. Some variation exists in the water table elevations for the studied wells in the Dibdibba region between summer and winter. The mean value of the variation for the considered wells is about 0.3 m. The mean values for the elevations of the water table of summer and winter were used in the simulation.

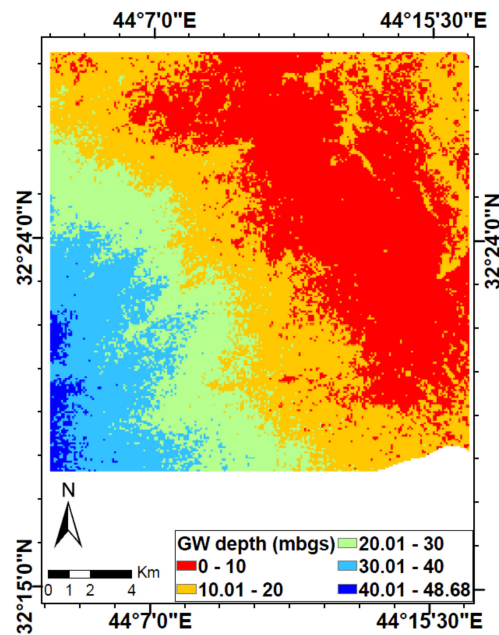


Figure 5. Groundwater table depth within Dibdibba study area (m.b.g.s.), modified after Al-Madhloom et al. (2019) [103].

As for the Babylon region, the climate of this region is arid to semi-arid. The annual average precipitation is about 100 mm/year. The mean annual temperature is about 24 °C. The temperature can exceed 50 °C during the day in summer and fall below 0 °C at night in winter. The mean annual evaporation ranges from 3.4 to 3.5 m/year [72,115].

3. Materials and Methods

This section is divided into three subsections: Theory and equations; ArcMap/GIS software; and Methodology. The first subsection outlines the theory and equations used in this article. The second subsection discusses the software used. Finally, the last subsection describes the methodology used in this study.

3.1. Theory and Equations

Seepage velocity refers to the velocity of flowing groundwater within the pores of the aquifer matrix [75]. It can be defined as “the rate of movement of fluid particles through porous media along a line from one point to another” [76]. It is an apparent velocity through the bulk of the porous medium [118]. Although it is an apparent velocity, it is more realistic than Darcy flux (misleadingly called Darcy velocity) for the expression of the actual velocity of groundwater within the pores of an aquifer; this is because the Darcy flux is fabricated and assumes that the flow occurs through the entire cross section of the soil, whereas in reality the flow is limited to the space of the pores [122]. The seepage velocity can be found by dividing the Darcy flux by the effective porosity, shown in Equation (1) [122,123]:

$$v_{seep} = \frac{v}{n_{eff}} \quad (1)$$

where v_{seep} is the seepage velocity (m/s), v is the Darcy flux ($\text{m}^3/\text{s}\cdot\text{m}^2$), and n_{eff} is the effective porosity of the aquifer (dimensionless). Darcy velocity is equal to the hydraulic gradient multiplied by the hydraulic conductivity of the aquifer, as in Equation (2) [73,123]:

$$v = -k \frac{\Delta h}{\Delta s} \quad (2)$$

where k is the hydraulic conductivity (m/s), Δh is the difference in the hydraulic head (m), and Δs is the distance (m). The hydraulic conductivity can be written in terms of transmissivity and the saturated thickness of the aquifer, as in Equation (3) [73,75]:

$$k = \frac{T}{b} \quad (3)$$

where T is the transmissivity (m²/s) and b is the saturated thickness of the aquifer (m).

Equation (3) is useful in groundwater hydraulics because most of the wells' hydraulic logs, calculations, and equations are written in terms of the transmissivity rather than the hydraulic conductivity [73,75], and because transmissivity is an aquifer or a well attribute, whereas hydraulic conductivity is a soil characteristic.

According to Equations (1)–(3), the seepage velocity can be written as Equation (4):

$$v_{seep} = -\frac{T}{b n_{eff}} \frac{\Delta h}{\Delta s} \quad (4)$$

Equation (4) was modeled in ArcMap/GIS and was used as a map framework to determine seepage velocity within the aquifers.

3.2. ArcMap/GIS Software

ArcMap/Geographic Information System (GIS), offered by Environmental Systems Research Institute (Esri), is powerful mapping software, which includes tools to create maps, perform spatial analysis, manage geographic data, and share results [124]. This software includes a tool called Darcy Velocity within the Spatial Analyst Tools\Groundwater box (Figure 6a). This tool is used to map seepage velocity. To draw seepage velocity using this tool, four raster maps are required to be inputted, they are (Figure 6b) [125,126]:

- groundwater elevation head;
- aquifer effective porosity;
- aquifer saturated thickness;
- aquifer transmissivity.

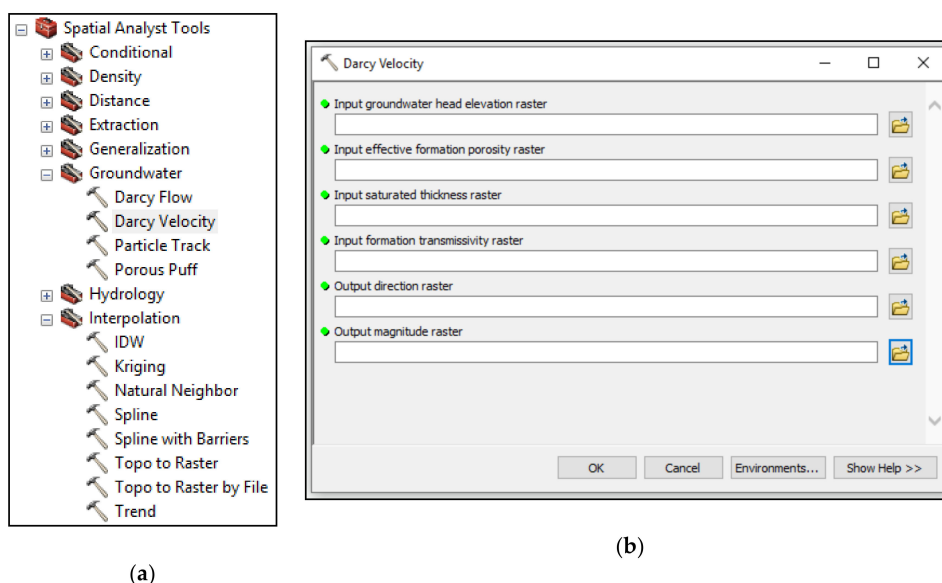


Figure 6. ArcMap/Geographic Information System (GIS) tools used: (a) interpolation; (b) Darcy velocity interface [109].

Three conditions must be fulfilled within the input raster maps so that they can be used to determine seepage velocity [125]:

- the rasters of the four maps must have the same extent and cell size;
- the rasters of the four maps must be a floating point;
- the maps should be dimensionally homogeneous, i.e., data should be consistent in units, using the same unit for time (years, days, seconds) and length (meters, feet) for all data.

Two output raster maps are produced: the seepage velocity magnitude and the seepage velocity direction (Figure 6b).

3.3. Methodology

The same methodology was used for both regions of the study area: Babylon and Dibdibba. The methodology was as follows. The required data were collected from the wells in the region. The collected data included: well locations (longitude and latitude); the static water head (m.b.g.s.) (meter below the ground surface, which represents the distance between the ground surface and the static water elevation in the well); transmissivity of the aquifers at the locations of the wells (m^2/d); effective porosity of the aquifer (dimensionless); and saturated thickness of the aquifers (m). The homogeneity of the units of the input data were considered during the data collection. Since the wells' logs did not state the effective porosity, the values of effective porosity at the well locations were obtained from internal reports of the Iraqi Ministry of Water Resources and Al-Qadisiyah University, Iraq (Table 1). Therefore, the actual effective porosity values taken in the field (and were used) were less than the suggested porosity cited in the literature, see [73] and Table 1. The range of the actual effective porosity and the total porosity are shown in Table 1.

Table 1. Actual effective porosity in the study area (obtained from the Iraqi Ministry of Water Resources and Al-Qadisiyah University, Iraq) compared with the total porosity stated in the literature.

Region	Actual Effective Porosity (as Percent)	Material	Total Porosity (as Percent), [73]
Babylon	21.9–26.2	Silt	46
		Clay	42
Dibdibba	23–29.3	Sandstone, medium grained	37

All of the acquired data were converted to Excel files, which were then exported to ArcMap/GIS. Then, the wells were projected using WGS1984UTM38N projection type and the well locations (latitude and longitude). WGS1984 refers to World Geodetic System 1984, UTM to Universal Transverse Mercator; 38 N is the area bounded by 42 E and 48 E, which includes most of the country of Iraq [127,128], i.e., the study area.

Next, four event layers were made by using the Excel table: static water level; transmissivity; effective porosity; and saturated thickness. Using a kriging-type interpolation tool (Figure 7a), the four event layers were converted to interpolated maps considering the raster cell sizes (which should be the same). Three of the four layers were directly used as inputs in the Darcy velocity command window (Figure 6b): transmissivity; effective porosity; and saturated thickness. The static water level map could not be used because the command window requires a groundwater head elevation (water table elevation) map rather than a static water elevation (water table depth) map. To resolve this issue, the Digital Elevation Map (DEM) for the study area was acquired. Then the static water level raster map was subtracted from the DEM raster map to obtain the groundwater head elevation map. Subtraction was performed using the Map Algebra/Raster calculator tool within Spatial Analyst Tools (Figure 7b). The resultant raster map was stored using a significant name.

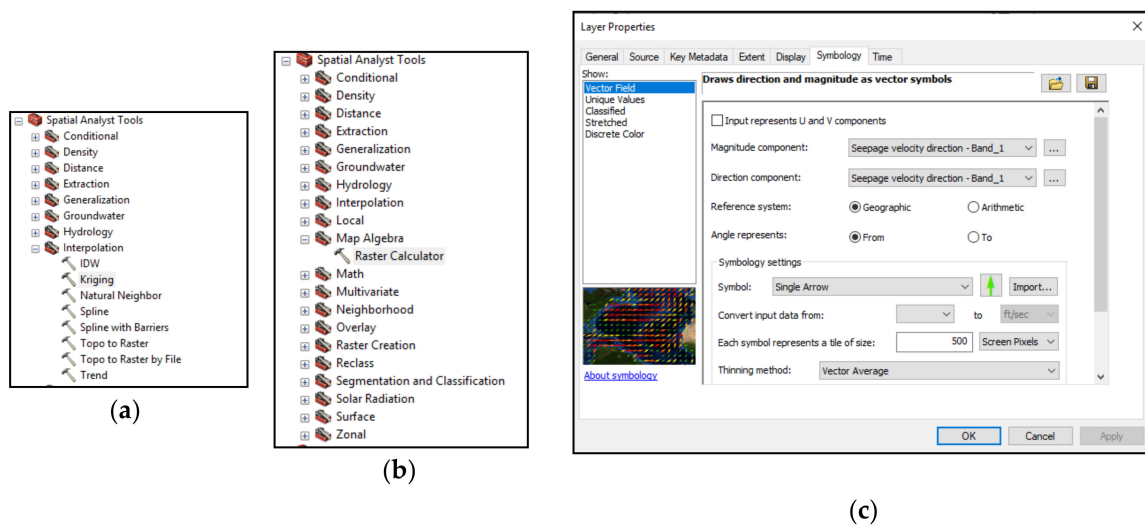


Figure 7. Additional tools and settings used: (a) interpolation tool, kriging type; (b) Map Algebra/Raster Calculator; (c) settings window for Darcy velocity direction map [109].

After producing the groundwater head elevation map, the inputs were completed and ready to be used in the Darcy velocity command window (Figure 6b). By inputting all of the required input maps and specifying the desirable paths of the output maps, the tool was used to produce both of the seepage velocity maps: magnitude and direction. The directional seepage velocity map needed to be reset by accessing “Symbology”; changing the “Show” style to “Vector Field”; and resetting the “Single Arrow” as “Symbol” (Figure 7c).

4. Results

The results can be divided into two parts in line with the considered region: Babylon (silty clayey aquifer), and Dibdibba region within Karbala province (sandy aquifer).

4.1. Babylon

As stated previously, the Darcy velocity tool requires inputting four raster layers (head, effective porosity, saturated thickness, and transmissivity) to produce the seepage velocity maps (magnitude and direction). The required data was collected from the wells’ logs, which were published in Al-Jiburi and Al-Basrawi (2011) [114]. The input layers were constructed as follows:

To draw the groundwater elevation map, an elective and typical reference is needed. In this study, the sea level was considered a datum for measuring the groundwater elevation. The study area has a graduated change in groundwater elevation from the northwest to the southeast. The groundwater level ranges from 38.27 m above sea level (m.a.s.l.) in the northern parts of the province to about 16 m.a.s.l. in the southern parts (Figure 8).

Data obtained from the in situ geo-hydrological surveys, gathered by the Iraqi Ministry of Water Resources and Al-Qadisiyah University (Iraq), was used to map the effective porosity within the regions of the study area. For the Babylon aquifer, the values of effective porosity ranged from 21.9% to 26.2%; see Figure 9. These values are less than those stated in the literature, which are 42% for clay and 46% for silt [73]; see Table 1 and Figure 9.

The saturated thickness represents the thickness of the aquifer surrounded by the water table and the bed of the aquifer. Because the wells’ logs included the values of both the water table and the aquifer bed, the saturated thickness was able to be calculated. The saturated thickness within the Babylon study area varies from 8.8 to 32.5 m; see Figure 10.

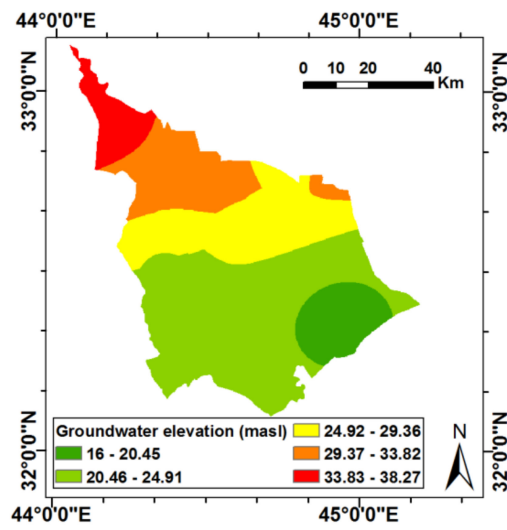


Figure 8. Groundwater elevation map within Babylon province.

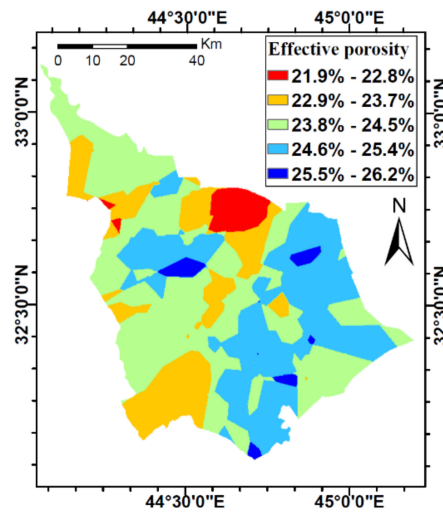


Figure 9. Actual effective porosity map for Babylon aquifer (obtained from the Iraqi Ministry of Water Resources and Al-Qadisiyah University, Iraq).

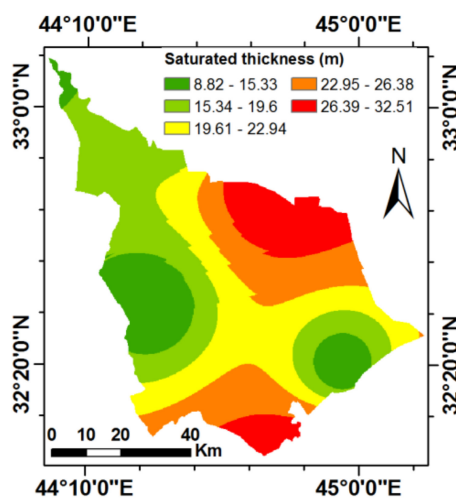


Figure 10. Saturated thickness map for Babylon aquifer, modified after [71].

Transmissivity can be defined as saturated thickness multiplied by hydraulic conductivity (Equation (3)). Therefore, its values depend on both saturated thickness and hydraulic conductivity. The region has a considerable graduated transmissivity from west to east. The transmissivity within the Babylon study area ranges from 52 to 157 m²/d (Figure 11). A general trend can be observed from the east to the west.

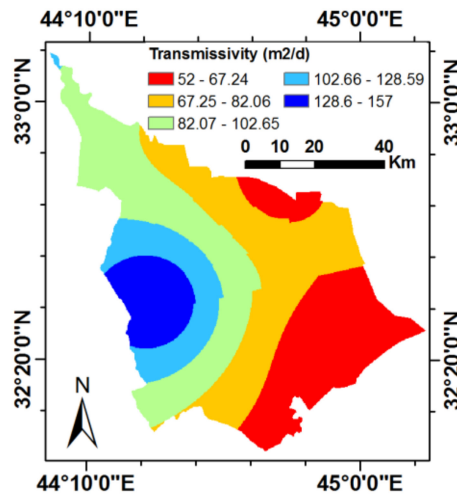


Figure 11. Transmissivity map for Babylon aquifer, modified after [71].

By inputting the four raster maps (hydraulic head, effective porosity, transmissivity, and saturated thickness) into the Darcy velocity command window (Figure 6b), seepage velocity maps were able to be produced. The resultant maps include: direction (Figure 12a), magnitude (Figure 12b), and merged (magnitude and direction) maps (Figure 12c). The results indicate that the groundwater in Babylon province flows from the north and the northwest to the south and the southeast (Figure 12a). The groundwater flow direction is consistent with the ground surface elevation and slope. Focusing on magnitude, the seepage velocity ranges from 2.12×10^{-6} to 0.185 m/day (Figure 12b). About 86% of the region has a seepage velocity ranging from 2.12×10^{-6} m/d to 5.09×10^{-3} m/d, and 12% between 5.10×10^{-3} and 1.74×10^{-2} m/d. The remainder of the region (about 2%) has a velocity ranging between 1.74×10^{-2} and 0.185 m/d.

The groundwater flow direction is consistent with the groundwater elevation. The groundwater flow from high to low head elevation within the region is shown in Figure 12d.

The map of the hydraulic gradient of groundwater can be used to examine the behavior of groundwater within the region. This map represents the slope of the water table (groundwater hydraulic gradient) within the Babylon aquifer. According to the equations, the groundwater hydraulic gradient is found by dividing the change in the elevation of the water table (ΔH) (Figure 8) by the distance (ΔS), i.e., $(\Delta H/\Delta S)$. Practically, it can be found by using the Slope tool within the ArcMap/GIS software. For the Babylon study area, the map is as shown in Figure 13. The hydraulic gradient is represented as a percent, and ranges from 0 to about 0.837% (8.37 m/km). By analyzing the hydraulic gradient map and comparing it with the seepage velocity magnitude map, it can be found that a fair match exists between the two maps. This is expected because the hydraulic gradient represents the driving force of the seepage velocity; see Equations (1), (2) and (4).

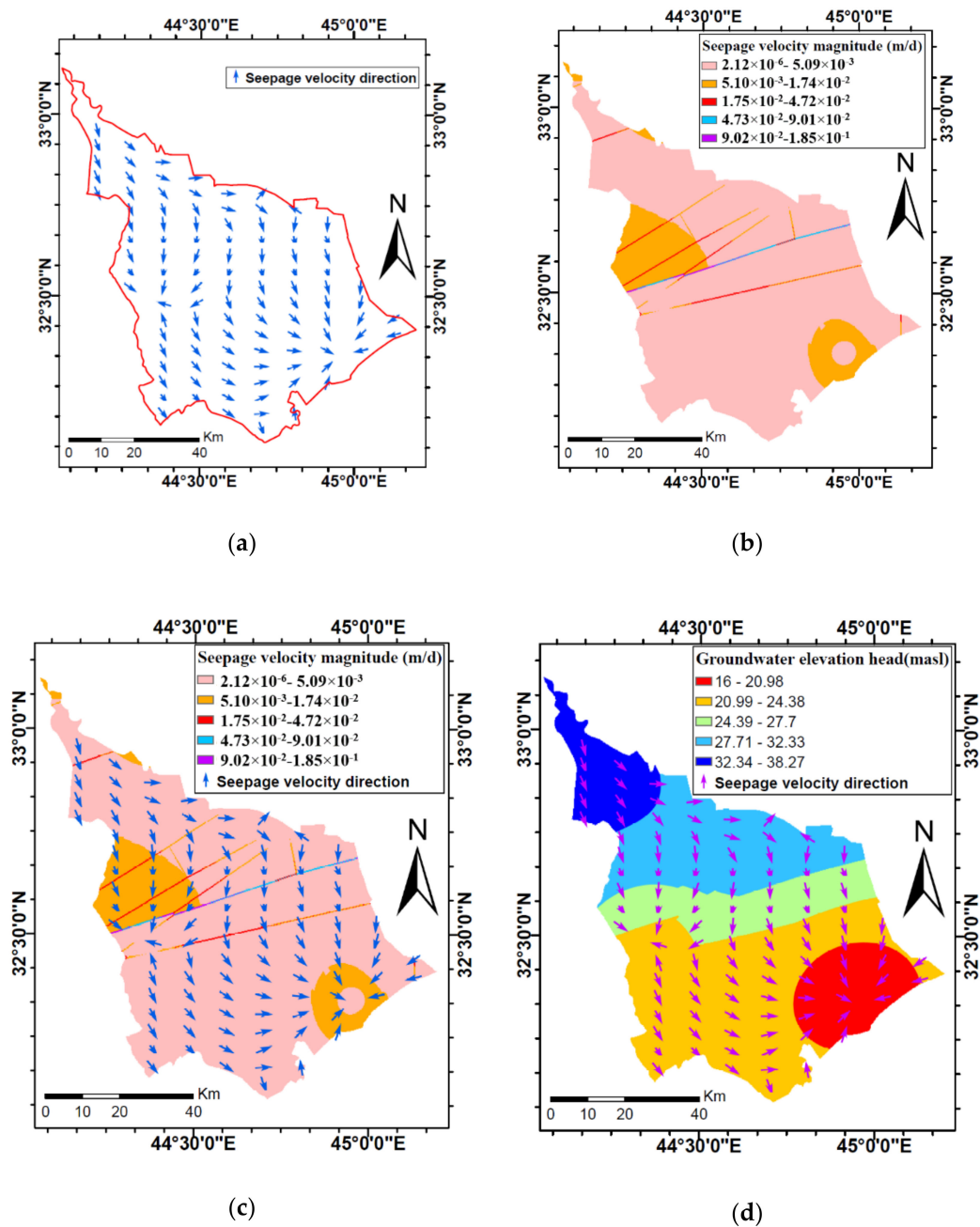


Figure 12. Seepage velocity maps for Babylon groundwater: (a) direction map; (b) magnitude map; (c) merged magnitude–direction map, (d) seepage direction–groundwater elevation head map.

4.2. Dibdibba Region

Where possible, required data were collected from well logs. In this study, however, required data were obtained from maps produced by Al-Ani [129]. Then, the obtained values were used to map the four fundamental maps that were required to produce the seepage velocity maps. The results for the four maps are as follows:

Groundwater elevation is graduated from west to east. It ranges from 40.2 m.a.s.l. in the western parts of the region to about 17.5 m.a.s.l. in the eastern parts (Figure 14). The difference in the elevation of the water table between the western and eastern parts was about 22.7 m. This difference is the source of the energy that causes the groundwater flow. The slope of the water table is consistent with the

slope of the ground surface and the bed of the aquifer (the upper surface of the Injana formation); see Figures 14 and 4b.

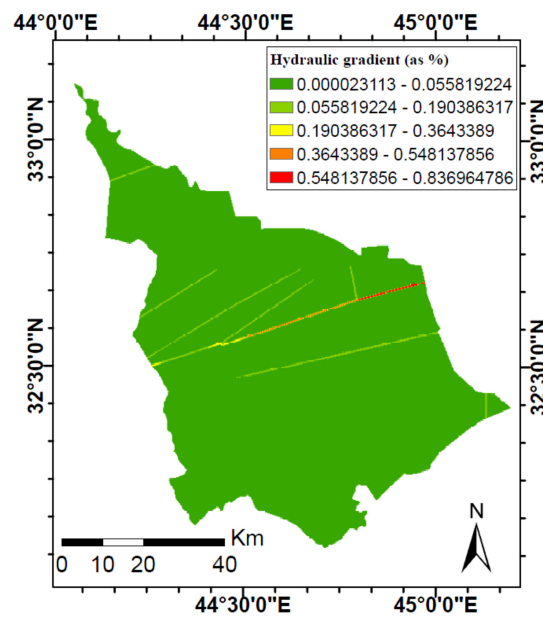


Figure 13. Groundwater hydraulic gradient in the Babylon study area.

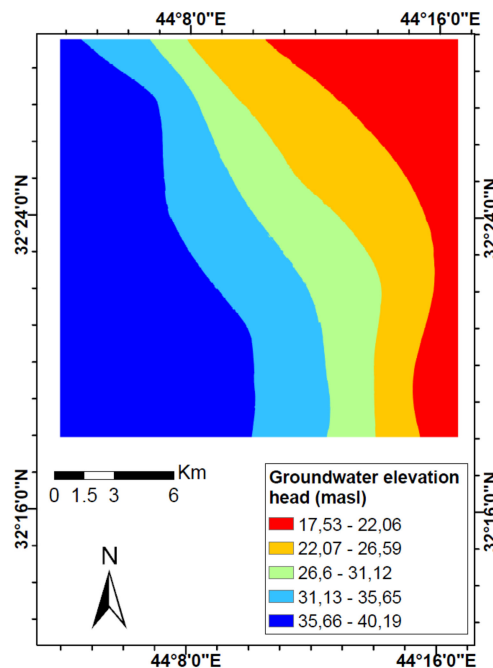


Figure 14. Groundwater elevation map within the Dibdibba region, modified after [120].

The effective porosity values, which were obtained from the Iraqi Ministry of Water Resources and Al-Qadisiyah University (Iraq), were used to map the effective porosity within the Dibdibba aquifer (Figure 15). The values of the actual effective porosity ranged from 23% to 29.3%. These values are less than the total porosity values stated in the literature; see Table 1 and Figure 15.

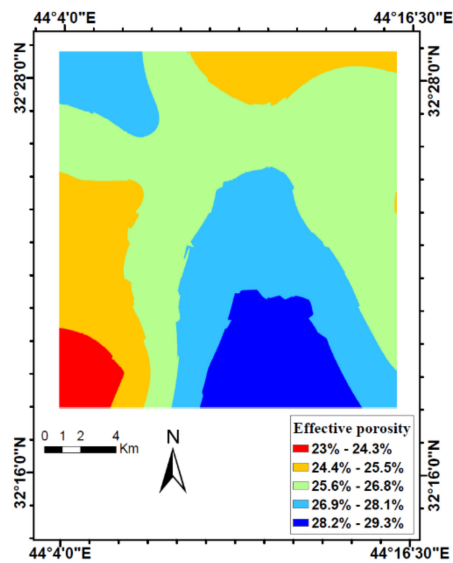


Figure 15. Actual effective porosity map for Dibdibba aquifer (data obtained from the Iraqi Ministry of Water Resources and Al-Qadisiyah University, Iraq).

The saturated thickness of the study area changes gradually from west to east, and ranges from 45.5 m in the western parts to 18.8 m in the eastern parts. The difference in the saturated thickness between the east and the west is about 26.7 m; see Figure 16a.

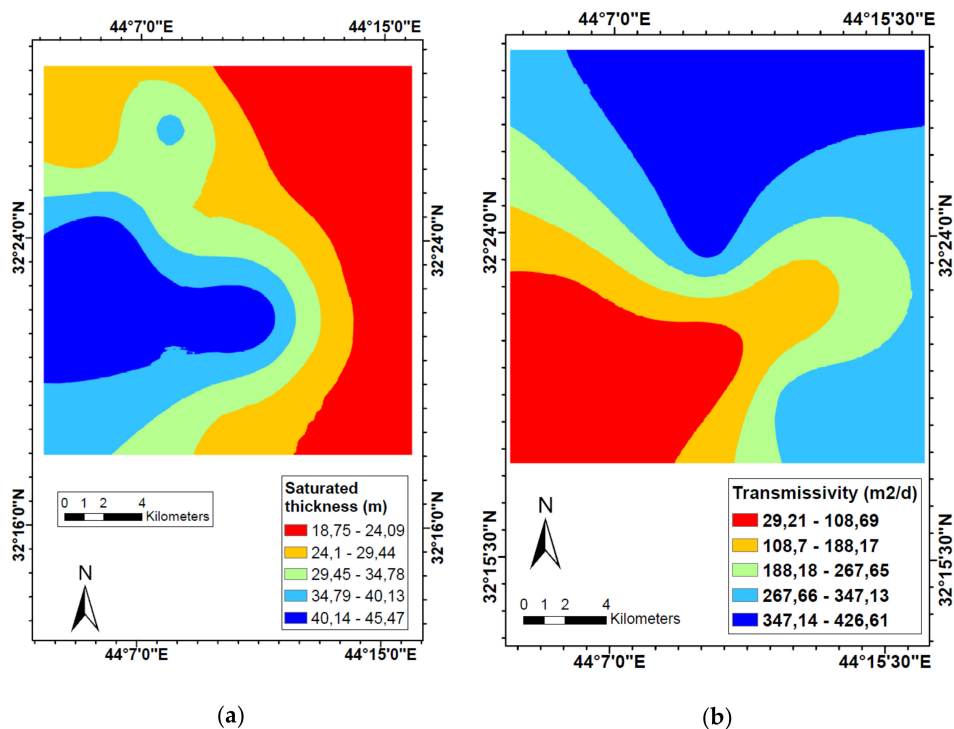


Figure 16. Maps of Babylon aquifer: (a) saturated thickness; (b) transmissivity of Babylon aquifer. Both maps are modified after [120].

Transmissivity is another property that showed a marked grading. It graduates from the southwest to the northeast direction, and ranges from 29.2 m²/d in the southwestern parts to 426.6 m²/d in the northeastern parts of the region (Figure 16b).

By inputting the four previous maps in the Darcy velocity command window and specifying the desirable paths of the output maps, the two seepage velocity maps (direction and magnitude) were able to be obtained. Considering the directional seepage velocity, it is clear that the groundwater flows in one direction, from west to east (Figure 17a). This direction is consistent with the bed of the aquifer and the groundwater elevation head. The magnitude of the seepage velocity ranges from 0 to about 0.27 m/day; see Figure 17b. About 28% of the region has a velocity between 0 and 1.92×10^{-2} m/d, 21% between 1.921×10^{-2} m/d and 4.58×10^{-2} m/d, 29% between 4.58×10^{-2} m/d and 7.67×10^{-2} m/d, 15% between 7.67×10^{-2} m/d and 0.114 m/d, and the remainder (about 6%) between 0.114 m/d and 0.272 m/d; see Figure 17b. The combined direction–magnitude map of seepage velocity is shown in Figure 17c.

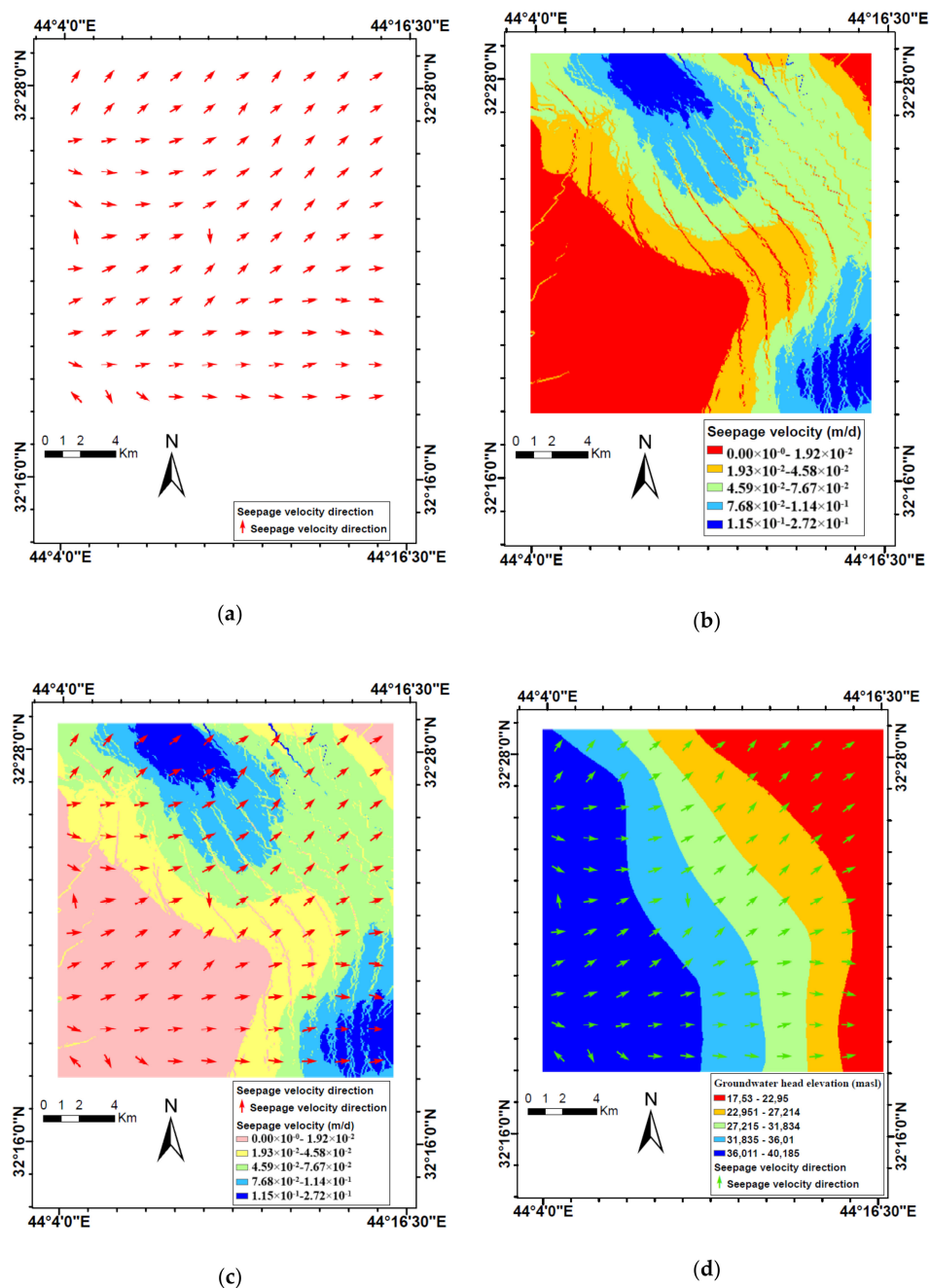


Figure 17. Seepage velocity map for Dibdibba groundwater: (a) direction map; (b) magnitude map; (c) merged magnitude–direction map; (d) seepage direction–groundwater elevation head map.

The groundwater flow direction is consistent with the groundwater elevation. The groundwater flow from high to low head elevation within the region is shown in Figure 17d.

The hydraulic gradient map for the groundwater in the Dibdibba study area is shown in Figure 18. It ranges from 0 to about 0.595 (5.95 m/km). Focusing on Figures 17b and 18, it can be noted that the hydraulic gradient and the seepage velocity magnitude maps have a fair match. The reason for this similarity is the same as that which explains the matching of the seepage velocity and the hydraulic gradient of the Babylon studied area.

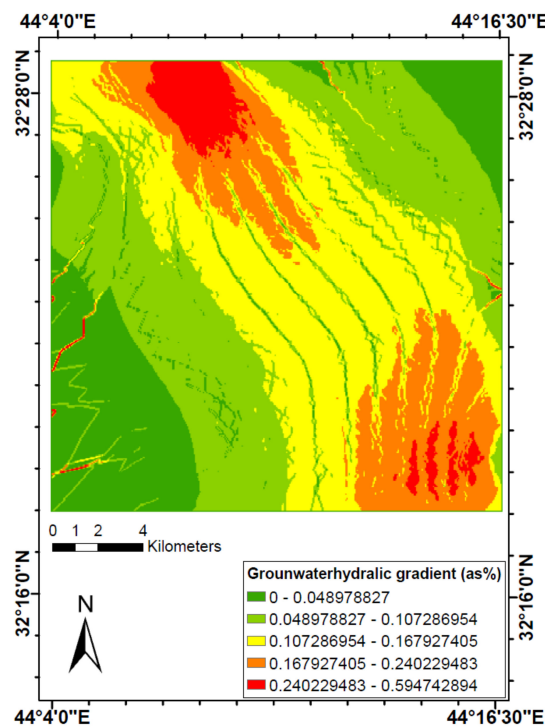


Figure 18. Groundwater hydraulic gradient in the Dibdibba study area.

By examining the maps of the hydraulic gradient of the two study areas (Babylon and Dibdibba) (Figures 13 and 18), it can be found that the range for Babylon is 0–8.37 m/km, and that for Dibdibba is 0–5.95 m/km. This means Babylon has a higher hydraulic gradient than the Dibdibba area. Despite the higher hydraulic gradient of Babylon compared to Dibdibba, the seepage velocity within Babylon (0.185 m/d) is less than that of Dibdibba (0.272 m/d). This is due to two geo-hydrological properties: First, the different compositions of the two aquifers (soil particle sizes for silty clayey loam and sand); second, the different structures of the two aquifers (effective porosity); see Figures 9 and 15. Both of these geo-hydrological properties affect the hydraulic conductivity of the two aquifers.

The comparison of the geo-hydrological properties of the two regions of the study area is summarized in Table 2. Table 2 provides the range (where available) of each geo-hydrological property; see Figures 8–18.

Table 2. Comparison of the geo-hydrological properties between Babylon and Dibdibba.

Property	Unit	Babylon	Dibdibba
Groundwater elevation	m.a.s.l.	16–38.27	17.53–40.19
Effective porosity range	%	21.9–26.2	23–29.3
Saturated thickness	m	8.82–32.51	18.75–45.47
Transmissivity	m ² /d	52–157	29.21–426.61
Hydraulic gradient	m/km	0–8.37	0–5.95
Seepage velocity magnitude	m/d	2.12×10^{-6} –0.185	0–0.272
Seepage velocity direction	-	Northwest to southeast	West to east

5. Discussion

Many researchers have studied the geo-hydrological properties of the two regions of the study area, but most did not specify the exact location (x and y coordinates, or longitude and latitude) in their studies. Rather than providing specific locations, they discussed region-wide ranged values, i.e., the data was not precise and lacked accuracy. Nonetheless, some researchers provided specific results concerning the geo-hydrological properties within a study area. These are discussed below, and their results are compared with the results of this article. The discussion section is divided into separate subsections for each of Dibdibba and Babylon.

5.1. Dibdibba Study Area

Jassim and Goff [113] stated in their book (Geology of Iraq) the depth of the water table for the whole of the country of Iraq. According to their results, the depth of the water table in the Dibdibba study area ranges between 5 and 20 m.b.g.s. Compared to the results of the current study (0–48 m.b.g.s.; Figure 5), there is a significant difference in the value of the upper limit. However, both studies suggest the same slope for the water table, from west to east; see Figure 14.

Al-Jiburi and Al-Basrawi (2007) studied the hydrology of the Western desert (which includes the Dibdibba study area) [130]. According to their results, the groundwater flows from the west to the east, which is similar to results of the current study; see Figure 17a,c,d [130].

Al-Mussawi (2008) used two GIS methods to estimate the groundwater elevation in the Dibdibba study area in two cases: dry (August 2002) and wet (March 2003) [131]. The GIS Tools used were kriging and inverse distance weighted (IDW). The values for the groundwater elevations using the kriging method ranged between 20 and 40 m.a.s.l. for the months of August 2002 and March 2003. These are approximately equal to the results of the current study for the groundwater elevations (17.5–40.2 m.a.s.l.); see Figure 14.

Al-Dabbas et al. [132] estimated transmissivity in the area neighboring the Dibdibba study area and calculated a range of 55.1–903 [132]. In the same paper, the authors determined the general direction of groundwater flow as being from the west to the east. Compared to the current study, a significant difference exists for the upper limit for transmissivity, with the current work estimating a range between 29.2 and 426.6 m²/d (see Figure 17). Regarding the flow direction, the two sets of results are consistent (see Figure 17a).

The research of Al-Jiburi and Al-Basrawi (2015) included a map of the groundwater flow direction within Iraq [115]. The direction of the groundwater flow within the Dibdibba study area was from the west to the east, which is consistent with the result of the current study; see Figure 17a.

Thabit and Khalid (2016) proved that the seepage direction in a small area (30 × 30 m) within the region of Dibdibba is from the west (more specifically, the southwest) to the east (more specifically, the northeast), which is consistent with the current results [133].

Al-Sudani (2018) estimated geo-hydrological properties for the Dibdibba region [134], including saturated thickness and transmissivity, deriving a range for saturated thickness of 10–40 m, and a range for transmissivity of 10–150 m²/d. This saturated thickness result is consistent with the corresponding result in the current work (see Figure 16a), whereas the transmissivity is less than that mapped in the present study (Figure 16b). However, both papers agree that the transmissivity increases in the same direction, from the southwest to the northeast (see Figure 16b).

Al-Abadi et al. [135] estimated the ranges of transmissivity and saturated thickness of the right edge of Dibdibba basin, including the study area of the current paper. These were 24–605 m²/d and 11.11–44.88 m, respectively; by comparison, the current work estimated a transmissivity range of 29.2–426.6 m²/d, and a saturated thickness range of 18.8–45.5 m. These results are consistent because the area investigated in the current study was included in the study area of [135].

In his study of the Iraq region, Al-Areedhi [136] found a range of groundwater elevation in the Dibdibba study area of 15 to 31 m.a.s.l., which is close to that of the current study (17.5–40.2 m.a.s.l.;

see Figure 14). The direction of the groundwater flow was similar to that in the current study, i.e., from the west to the east (see Figure 17a).

Saleh et al. [137] studied the groundwater for the whole of Iraq. They estimated the range of transmissivity values within the cone-shaped Dibdibba basin, which includes the Dibdibba study area, as 29.2–426.6 m²/d. This is precisely the same range that was estimated in the current study; see Figure 16b. The same authors estimated the direction of the groundwater flow within Dibdibba study area; it was from the west to the east.

No previous studies estimated the effective porosity, hydraulic gradient, and seepage velocity magnitude in the Dibdibba study area. In addition, we could not find any previously published materials about the field values of these geo-hydrological properties within the Dibdibba study area, with the exception of interior reports produced by the Iraqi Ministry of Water Resources and Al-Qadisiyah University (Iraq) that included values for effective porosity.

5.2. Babylon Study Area

Although a small number of publications exist concerning the seepage velocity within Dibdibba study area, the number of publications about the Babylon region is even fewer. This is because of the dependence on surface water (the Euphrates River) rather than groundwater in the Babylon region, and is in contrast with the Dibdibba study area, in which there is greater reliance on groundwater due to a lack of surface water.

Furthermore, few studies have examined the geo-hydrological properties investigated in this article for the Babylon area. The results acquired in previous research are generally limited to groundwater elevation and direction of the groundwater flow. Few examinations have been made of transmissivity and saturated thickness, and almost no data gathered on effective porosity, with the exception of the interior report produced by the Iraqi Ministry of Water Resources and Al-Qadisiyah University (Iraq).

In their book, Jassim and Goff [113] estimated the depth of the water table in the Babylon study area [113], finding that it ranged between 1 and 5 m.b.g.s. This is similar to the results of the current study, which estimated a range of 1–9 m.b.g.s. (Figure 3). Furthermore, both sets of results indicated the same direction for the groundwater elevation decrement, i.e., from northwest to southeast (see Figure 8).

Al-Jiburi and Al-Basrawi [114] published a paper concerning the hydrogeology and large morphology of Mesopotamia Plain, which includes the Babylon study area. The authors divided the Mesopotamia Plain into three regions: northern, central, and southern. According to [114], the range of transmissivity in the Babylon area is 10–165 m²/d, which is consistent with the results of the current study (52–157 m²/d; see Figure 11). In the same paper, the authors mapped the groundwater flow direction from northwest to southeast, which is also consistent with the results of this work (see Figure 12a). In 2015, the same authors published another paper [115], in which they confirmed the results of the previous paper [114] regarding the groundwater flow direction in Babylon (i.e., northwest to southeast).

Al-Ansari et al. [138] studied the groundwater in Iraq, including maps of the flow direction. The results are consistent with the findings of the current study, with both papers stating that the groundwater flows from the northwest to the southeast (see Figure 12a).

Al Maimuri [139] examined groundwater table elevation, saturated thickness, transmissivity, and seepage velocity within the Hashimiya region, which is located within the Babylon study area, and estimated ranges for each of groundwater level and transmissivity; these were 21–25 m.a.s.l. and 250–420 m²/d, respectively. The groundwater elevation range is similar to that of the current work because Hashimiya is in the southern part of Babylon, i.e., within the ranges of 16–20.5 m.a.s.l. and 20.5–24.9 m.a.s.l. shown on the groundwater elevation map (see Figure 8). Regarding transmissivity, the results for the Hashimiya region range between 52 and 102 m²/d, compared to the results of the current study, which extend across three classes of transmissivity, i.e., 52–67.2 to 82.2–102.7 (Figure 11). There is thus a significant difference between the two results. The estimated values for the

seepage velocity from the two papers are consistent, since they are within the ranges of 2.84×10^{-3} to 3.29×10^{-3} m/d for [139] and 1.34×10^{-6} to 3.45×10^{-3} m/d for the current work.

Based on the comparisons outlined above for both regions of the study area (Dibdibba and Babylon), the results of the current paper appear to be broadly consistent with those of previous research. Furthermore, the results of the current study are important due to the lack of knowledge regarding the investigated geo-hydrological properties for the two studied regions.

6. Conclusions

Arc Map/GIS provides a suitable tool (Darcy velocity) to determine the seepage velocity and depict the results as large-scale maps. Accuracy of the resultant seepage velocity maps depends on the resolution of the four necessary underlying maps: groundwater elevation head; transmissivity; saturated thickness; and effective porosity. Thus, the accuracy of the resultant maps depends on the locations of the wells that are used to collect the data. In the case of complex topography, e.g., a mountainous area, more wells are required to reflect the real conditions of the topography and the geo-hydrological properties of the region.

Results of the current study showed that the groundwater in Babylon province flows from the northwest to the southeast. The seepage velocity direction is controlled by groundwater gradient. The seepage velocity in Babylon province is limited to 0.185 m/d.

In the Dibdibba formation, groundwater flows from the west to the east, with a velocity reaching 0.272 m/d. The difference in the velocities between the two aquifers is due to differences in the studied geological properties.

Although the Babylon region has a higher hydraulic gradient than Dibdibba, Dibdibba has higher seepage velocity. This is mainly due to the high hydraulic conductivity of the Dibdibba aquifer compared to that of the Babylon aquifer. A further explanation is the structure (effective porosity) and composition (size of particles) of the two aquifers.

Due to the importance of seepage velocity in heat/mass transfer applications, primary investigations must be conducted before initiating the construction of related infrastructure. These studies should include large-scale mapping of the seepage velocity to acquire a comprehensive understanding of the behavior of the groundwater within the considered region. This capability is provided by the ArcMap/GIS software.

Furthermore, the results of seepage velocity are useful in the design of landfill and ATEs systems. In the case of the installation of ATEs systems, for example, interference between cold and warm well storage should be minimized to prevent the energy losses. As a result, the planning of thermal energy storage wells should be perpendicular to the direction of groundwater flow. In Babylon, the axis between the warm and cold wells should extend from the southwest towards the northeast (perpendicular to the flow direction), and for Dibdibba it should extend from the north to the south (perpendicular to the east–west direction). In landfill planning, high seepage velocity regions should be excluded from the design to decrease the risk of contaminant spread in case of leakage.

Author Contributions: Conceptualization, Q.A.-M.; N.A.-A., J.L., and H.M.H.; methodology, Q.A.-M.; software, Q.A.-M.; validation, Q.A.-M. and N.A.-A.; formal analysis, Q.A.-M. and B.A.H.; investigation, Q.A.-M.; data curation, Q.A.-M.; writing—original draft preparation, Q.A.-M., N.A.-A., J.L., B.A.H. and H.M.H.; Project management, N.A.-A.; writing—review and editing, Q.A.-M., N.A.-A., J.L.; B.A.H., and H.M.H.; visualization, Q.A.-M. and N.A.-A.; supervision, N.A.-A., J.L. and H.M.H.; All authors have read and agreed to the published version of the manuscript.

Funding: University of Babylon granted a scholarship to the first author to do his PhD at Lulea University of Technology.

Acknowledgments: The authors would like to thank H.E. Mohammad Dhari, the Scientific Consultant of the Iraqi Ministry of Water Resources, and Salwan Ali for providing us with the actual effective porosity values of the study area.

Conflicts of Interest: The authors declare no conflict of interest.

References

1. Martin, J.L.; Maris, V.; Simberloff, D.S. The need to respect nature and its limits challenges society and conservation science. *Proc. Natl. Acad. Sci. USA* **2016**, *113*, 6105–6112. [CrossRef]
2. World Economic Forum. The Global Risks Report 2017 (12th Edition). Available online: http://www3.weforum.org/docs/GRR17_Report_web.pdf (accessed on 1 July 2020).
3. Voulvoulis, N.; Burgman, M.A. The contrasting roles of science and technology in environmental challenges. *Crit. Rev. Environ. Sci. Technol.* **2019**, *49*, 1079–1106. [CrossRef]
4. Krämer, L. *Global Environmental Challenges and the EU*; ERA Forum; Springer: Berlin/Heidelberg, Germany, 2019.
5. Nazarova, Y.A.; Sopilko, N.Y.; Kovaleva, E.A.; Kulakov, A.V.; Orlova, A.F.; Gavlovskaya, G.V. How to solve water shortage problem by means of renewable power generation? *Int. J. Energy Econ. Policy* **2019**, *9*, 244–249.
6. Falkenmark, M.; Lindh, G. *Water for a Starving World*; Routledge: New York, NY, USA, 1976.
7. Dwianika, A.; Murwaningsari, E.; Suparta, W. Analysis of water awareness, accountability, and governance to improve sustainability of firm's performance in urban areas. *Geogr. Tech.* **2020**, *15*, 39–50.
8. (WRI) WRI. Water. Available online: <https://www.wri.org/our-work/topics/water> (accessed on 5 June 2020).
9. NASA. Freshwater Stores Shrank in Tigris-Euphrates Basin. Available online: <https://earthobservatory.nasa.gov/images/80613/freshwater-stores-shrank-in-tigris-euphrates-basin> (accessed on 5 June 2020).
10. Voss, K.A.; Famiglietti, J.S.; Lo, M.; De Linage, C.; Rodell, M.; Swenson, S.C. Groundwater depletion in the Middle East from GRACE with implications for transboundary water management in the Tigris-Euphrates-Western Iran region. *Water Resour. Res.* **2013**, *49*, 904–914. [CrossRef]
11. World of Change: Mesopotamia Marshes. Available online: <https://earthobservatory.nasa.gov/world-of-change/iraq.php> (accessed on 5 June 2020).
12. Drought in Iraq. Available online: <https://earthobservatory.nasa.gov/images/38914/drought-in-iraq> (accessed on 5 June 2020).
13. United States Department of Agriculture USDA (Foreign Agricultural Service). *IRAQ: Drought Reduces 2008/09 Winter Grain Production*; United States Department of Agriculture USDA (Foreign Agricultural Service): Washington, DC, USA, 2008.
14. The Water Cycle. NASA. Available online: <https://earthobservatory.nasa.gov/features/Water/page1.php> (accessed on 5 June 2020).
15. Famiglietti, J.S. The global groundwater crisis. *Nat. Clim. Chang.* **2014**, *4*, 945–948. [CrossRef]
16. Kundzewicz, Z.W.; Döll, P. Will groundwater ease freshwater stress under climate change? *Hydrol. Sci. J.* **2009**, *54*, 665–675. [CrossRef]
17. Voss, K.; Swenson, S.; Rodell, M.; Richey, A.S.; Thomas, B.F.; Lo, M.H.; Reager, J.T.; Famiglietti, J.S. Quantifying renewable groundwater stress with GRACE. *Water Resour. Res.* **2015**, *51*, 5217–5238.
18. Alexandra, S.R.; Thomas, B.F.; Lo, M.H.; Famiglietti, J.S.; Swenson, S.; Rodell, M. Uncertainty in global groundwater storage estimates in a Total Groundwater Stress framework. *Water Resour. Res.* **2015**, *51*, 5198–5216.
19. Huang, F.; Zhang, Y.; Zhang, D.; Chen, X. Environmental groundwater depth for groundwater-dependent terrestrial ecosystems in arid/semiarid regions: A review. *Int. J. Environ. Res. Public Health* **2019**, *16*, 763. [CrossRef]
20. NASA. Study: Third of Big Groundwater Basins in Distress. Available online: <https://www.jpl.nasa.gov/news/news.php?feature=4626> (accessed on 5 June 2020).
21. Wang, Z.; Yang, L.; Sun, N. Research on optimal design of slope anti-seepage. *IOP Conf. Ser. Earth Environ. Sci.* **2019**, *304*, 1–5. [CrossRef]
22. Wang, L.; Wu, C.; Gu, X.; Liu, H.; Mei, G.; Zhang, W. Probabilistic stability analysis of earth dam slope under transient seepage using multivariate adaptive regression splines. *Bull. Eng. Geol. Environ.* **2020**, *79*, 2763–2775. [CrossRef]
23. Li, T.; Liu, G.; Wang, C.; Wang, X.; Li, Y. The Probability and Sensitivity Analysis of Slope Stability Under Seepage Based on Reliability Theory. *Geotech. Geol. Eng.* **2020**, *38*, 3469–3479. [CrossRef]
24. Han, Z.; Chen, X.; Huang, Y.; Luo, B.; Xing, H.; Huang, Y. Effect of slope gradient on the subsurface water flow velocity of sand layer profile. *J. Mt. Sci.* **2020**, *17*, 641–652. [CrossRef]

25. Liu, J.; Chen, Z.; Kanungo, D.P.; Song, Z.; Bai, Y.; Wang, Y.; Li, D.; Qian, W. Topsoil reinforcement of sandy slope for preventing erosion using water-based polyurethane soil stabilizer. *Eng. Geol.* **2019**, *252*, 125–135. [[CrossRef](#)]
26. Liu, G.; Zheng, F.; Jia, L.; Jia, Y.; Zhang, X.; Hu, F.; Zhang, J. Interactive effects of raindrop impact and groundwater seepage on soil erosion. *J. Hydrol.* **2019**, *578*, 124066. [[CrossRef](#)]
27. Qiu, P.T.; Chen, Z.Q.; Pu, H.; Zhang, L.Y. Non-Darcian seepage stability analysis of non-Newtonian fluid. *Therm. Sci.* **2019**, *23*, 1393–1399. [[CrossRef](#)]
28. Chouireb, M.; Djehiche, A. Simulation of seepage flow through an earthen dam with vertical drain and comparison of results with observations data (case study: Harreza dam-Algeria). *Arab. J. Geosci.* **2019**, *12*, 406. [[CrossRef](#)]
29. Asmaranto, R.; Priyantoro, D.; Rini, D.Y.; Aini, A.K. Safety evaluation of the existing Grawan dam based on hydro-geotechnical behaviour conditions to ensure the availability of water resources. *IOP Conf. Ser. Earth Environ. Sci.* **2020**, *437*, 012006. [[CrossRef](#)]
30. Ren, J.; Zhang, W.; Yang, J. Morris sensitivity analysis for hydrothermal coupling parameters of embankment dam: A case study. *Math. Probl. Eng.* **2019**, *2019*, 2196578. [[CrossRef](#)]
31. Li, H.; Zhao, F.; Li, J. Seepage analysis of clay core wall dam based on ABAQUS. *IOP Conf. Ser. Earth Environ. Sci.* **2019**, *384*, 012015. [[CrossRef](#)]
32. Kacimov, A.R.; Yakimov, N.D.; Šimůnek, J. Phreatic seepage flow through an earth dam with an impeding strip. *Comput. Geosci.* **2020**, *24*, 17–35. [[CrossRef](#)]
33. Sidiropoulos, P.; Tziatzios, G.; Vasiliades, L.; Mylopoulos, N.; Loukas, A. Groundwater nitrate contamination integrated modeling for climate and water resources scenarios: The case of Lake Karla over-exploited aquifer. *Water* **2019**, *11*, 1201. [[CrossRef](#)]
34. Li, Y.; Luo, Y. Application of Computational Fluid Dynamics in Groundwater Pollution Remediation. *J. Phys. Conf. Ser.* **2019**, *1300*, 012070. [[CrossRef](#)]
35. Agarwal, R.; Yadav, M.P.; Agarwal, R.P.; Goyal, R. Analytic solution of fractional advection dispersion equation with decay for contaminant transport in porous media. *Mat. Vesn.* **2019**, *71*, 5–15.
36. Siddiqui, D.A.; Peltier, E.F.; Young, B.; Sullivan, P.L. Modelling Influent Runoff and Retention Time in Storm Water Wetland Systems. In *World Environmental and Water Resources Congress 2019*; ASCE Library: Reston, VA, USA, 2019; pp. 400–410.
37. Li, Z.; Chen, J.; Sugimoto, M.; Ge, H. Numerical simulation model of artificial ground freezing for tunneling under seepage flow conditions. *Tunn. Undergr. Space Technol.* **2019**, *92*, 103035. [[CrossRef](#)]
38. Li, Z.; Chen, J.; Sugimoto, M.; Mao, C. Thermal Behavior in Cross-Passage Construction during Artificial Ground Freezing: Case of Harbin Metro Line. *J. Cold Reg. Eng.* **2020**, *34*, 1–13. [[CrossRef](#)]
39. Uprety, M.; Ochoa-Tocachi, B.F.; Paul, J.D.; Regmi, S.; Buytaert, W. Improving water resources management using participatory monitoring in a remote mountainous region of Nepal. *J. Hydrol. Reg. Stud.* **2019**, *23*, 100604. [[CrossRef](#)]
40. Jaiswal, R.K.; Yadav, R.N.; Lohani, A.K.; Tiwari, H.L.; Yadav, S. Water balance modeling of Tandula (India) reservoir catchment using SWAT. *Arab. J. Geosci.* **2020**, *13*, 148. [[CrossRef](#)]
41. Li, Z.; Gui, J.; Wang, X.; Feng, Q.; Zhao, T.; Ouyang, C.; Guo, X.; Zhang, B.; Shi, Y. Water resources in inland regions of central Asia: Evidence from stable isotope tracing. *J. Hydrol.* **2019**, *570*, 1–16. [[CrossRef](#)]
42. Liu, Q.; Hanati, G.; Danierhan, S.; Zhang, Y.; Zhang, Z. Simulation of Groundwater Level in Ephemeral Streams with an Improved Groundwater Hydraulics Model. *Groundwater* **2019**, *57*, 969–979. [[CrossRef](#)] [[PubMed](#)]
43. Ren, J.; Cheng, J.; Zhang, W.; Yang, J.; Zhou, Y.; Men, L.; Dai, J. Vertical fluid flux in the hyporheic zone: Field investigation, model, and comparative analysis. *Arab. J. Geosci.* **2020**, *13*, 1–14. [[CrossRef](#)]
44. Lewandowski, J.; Meinikmann, K.; Krause, S. Groundwater—Surface Water Interactions: Recent Advances and Interdisciplinary Challenges. *Water* **2020**, *12*, 296. [[CrossRef](#)]
45. Ma, D.; Wang, J.; Li, Z. Effect of particle erosion on mining-induced water inrush hazard of karst collapse pillar. *Environ. Sci. Pollut. Res.* **2019**, *26*, 19719–19728. [[CrossRef](#)]
46. Yang, B.; Yang, T.; Xu, Z.; Liu, H.; Yang, X.; Shi, W. Impact of particle-size distribution on flow properties of a packed column. *J. Hydrol. Eng.* **2019**, *24*, 1–11. [[CrossRef](#)]
47. Zhang, B.Y.; Lin, Z.B. Seepage Property of Crushed Mudstone Rock in Collapse Column. *Adv. Civ. Eng.* **2020**, *2020*, 1–10. [[CrossRef](#)]

48. Zhang, W.; Zhang, L.; Cui, P.; Gao, Y.; Liu, J.; Yu, M. Investigation of the influence of groundwater seepage on the heat transfer characteristics of a ground source heat pump system with a 9-well group. In *Building Simulation*; Tsinghua University Press: Beijing, China, 2019; Volume 12, pp. 857–868.
49. Wang, R.; Yang, C.; Ni, L.; Yao, Y. Experimental study on heat transfer of soil with different moisture contents and seepage for ground source heat pump. *Indoor Built Environ.* **2020**, *29*, 1–11. [[CrossRef](#)]
50. Gossler, M.A.; Bayer, P.; Zosseder, K. Experimental investigation of thermal retardation and local thermal non-equilibrium effects on heat transport in highly permeable, porous aquifers. *J. Hydrol.* **2019**, *578*, 124097. [[CrossRef](#)]
51. Liu, X.; Li, W.; Liu, J.; Li, S.; Li, J. Experimental study of influence factors on heat transfer characteristics of brine aquifer. *Appl. Therm. Eng.* **2019**, *146*, 495–504. [[CrossRef](#)]
52. Chen, J.; Xiong, F.; Zheng, J.; Ge, Q.; Cheng, F. The influence of infiltration angle on the identification effect of seepage with linear heat source method. *Meas. J. Int. Meas. Confed.* **2019**, *148*, 106974. [[CrossRef](#)]
53. Huang, Y.; Zhang, Y.; Yu, Z.; Ma, Y.; Zhang, C. Experimental investigation of seepage and heat transfer in rough fractures for enhanced geothermal systems. *Renew. Energy* **2019**, *135*, 846–855. [[CrossRef](#)]
54. Luo, Z.; Xu, H. Numerical simulation of heat and mass transfer through microporous media with lattice Boltzmann method. *Therm. Sci. Eng. Prog.* **2019**, *9*, 44–51. [[CrossRef](#)]
55. Zhang, W.; Zhang, L.; Gao, Y.; Gao, X.; Zhang, H.; Yu, M. The annual fluctuation of underground temperature response caused by ground heat exchanger in the condition of groundwater seepage. *Energy Build.* **2019**, *186*, 37–45. [[CrossRef](#)]
56. Jiang, Y.; Wang, X.; Li, M.; Gao, Q. Investigations on heat flow characteristics of the aquifer for groundwater heat pump (GWHP) composed of different well types. *Int. J. Green Energy* **2019**, *16*, 857–866. [[CrossRef](#)]
57. Zhou, X.; Gao, Q.; Chen, X.; Yu, M.; Zhao, X. Numerically simulating the thermal behaviors in groundwater wells of groundwater heat pump. *Energy* **2013**, *61*, 240–247. [[CrossRef](#)]
58. Klepikova, M.; Wildemeersch, S.; Hermans, T.; Jamin, P.; Orban, P.; Nguyen, F.; Brouyère, S.; Dassargues, A. Heat tracer test in an alluvial aquifer: Field experiment and inverse modelling. *J. Hydrol.* **2016**, *540*, 812–823. [[CrossRef](#)]
59. Wildemeersch, S.; Jamin, P.; Orban, P.; Hermans, T.; Klepikova, M.; Nguyen, F.; Brouyère, S.; Dassargues, A. Coupling heat and chemical tracer experiments for estimating heat transfer parameters in shallow alluvial aquifers. *J. Contam. Hydrol.* **2014**, *169*, 90–99. [[CrossRef](#)]
60. Fleuchaus, P.; Godschalk, B.; Stober, I.; Blum, P. Worldwide application of aquifer thermal energy storage—A review. *Renew. Sustain. Energy Rev.* **2018**, *94*, 861–876. [[CrossRef](#)]
61. Vonsée, B.; Crijns-Graus, W.; Liu, W. Energy technology dependence—A value chain analysis of geothermal power in the EU. *Energy* **2019**, *178*, 419–435. [[CrossRef](#)]
62. Kumari, W.G.; Ranjith, P.G. Sustainable development of enhanced geothermal systems based on geotechnical research—A review. *Earth-Sci. Rev.* **2019**, *199*, 102955. [[CrossRef](#)]
63. Şen, Z. Innovative methodologies in renewable energy: A review. *Int. J. Energy Res.* **2019**, *43*, 5621–5658. [[CrossRef](#)]
64. Tsagarakis, K.P.; Efthymiou, L.; Michopoulos, A.; Mavragani, A.; Anđelković, A.S.; Antolini, F.; Bacic, M.; Bajare, D.; Baralis, M.; Bogusz, W.; et al. A review of the legal framework in shallow geothermal energy in selected European countries: Need for guidelines. *Renew. Energy* **2020**, *147*, 2556–2571. [[CrossRef](#)]
65. Hoekstra, N.; Pellegrini, M.; Bloemendal, M.; Spaak, G.; Gallego, A.A.; Comins, J.R.; Grotenhuis, T.; Picone, S.; Murrell, A.J.; Steeman, H.J.; et al. Increasing market opportunities for renewable energy technologies with innovations in aquifer thermal energy storage. *Sci. Total Environ.* **2020**, *709*, 136–142. [[CrossRef](#)]
66. Halaj, E.; Kepinska, B. Conjunctive uses of the geothermal water resources from lower cretaceous formations in the Mogilno–Lodz trough; Poland. *Sustain. Water Resour. Manag.* **2019**, *5*, 1479–1494. [[CrossRef](#)]
67. Mannah, M.A.; Makki, L.; Haddad, A.; Bazzi, H. Renewable Energy Technologies Penetration in MENA Region (2010–2030). *J. Electr. Eng.* **2016**, *4*, 99–107.
68. IEA. *Renewables 2019, Market Analysis and Forecast from 2019 to 2024*; IEA: Paris, France, 2019; pp. 1–7.
69. Cetin, A.; Kadioglu, Y.K.; Paksoy, H. Underground thermal heat storage and ground source heat pump activities in Turkey. *Sol. Energy* **2020**, *200*, 22–28. [[CrossRef](#)]
70. Al-Kayiem, H.H.; Mohammad, S.T. Potential of renewable energy resources with an emphasis on solar power in Iraq: An outlook. *Resources* **2019**, *8*, 42. [[CrossRef](#)]

71. Al-Madhloom, Q.; Al-Ansari, N.; Laue, J.; Nordell, B.; Hussain, H.M. Site selection of aquifer thermal energy storage systems in shallow groundwater conditions. *Water* **2019**, *11*, 1393. [CrossRef]
72. Al-Madhloom, Q.; Nordell, B.; Chabuk, A.; Al-Ansari, N.; Lindblom, J.; Laue, J.; Hussain, H.M. Potential use of UTES in Babylon Governorate, Iraq. *Groundw. Sustain. Dev.* **2020**, *10*, 100283. [CrossRef]
73. Todd, D.K.; Mays, L.W. *Groundwater Hydrology*, 3rd ed.; John Wiley & Sons, Inc.: Hoboken, NJ, USA, 2005.
74. Kovalevsky, V.S.; Kruseman, G.P.; Rushton, K.R. *Groundwater Studies: An International Guide for Hydrogeological Investigations*; UNESCO: Paris, France, 2004.
75. Delleur, J.W. (Ed.) *The Handbook of Groundwater Engineering*, 2nd ed.; Crc Press Inc., Taylor & Francis Group, LLC: New York, NY, USA, 2007.
76. Fetter, C.W.J. *Applied Hydrogeology*, 4th ed.; Pearson Education Limited: Harlow, UK, 2014.
77. Fetter, C.W.; Boving, T.; Kremer, D. *Contaminant Hydrogeology*, 3rd ed.; Waveland Press, Inc.: Long Grove, IL, USA, 2018.
78. Hiscock, K.M.; Bense, V.F. *Hydrogeology: Principles and Practice*, 2nd ed.; Wiley & Sons Ltd.: West Sussex, UK, 2014.
79. Rahmane, A.; Bentafat, A. Reality and prospect of electricity production from renewable energies in Arab countries: Analytical study (1990–2017). *Int. J. Energy Econ. Policy* **2018**, *8*, 39–47.
80. Renewable Energy Potential in the Arab Region. Available online: <https://www.eolss.net/Sample-Chapters/C08/E6-106-46.pdf> (accessed on 4 June 2020).
81. Bhutto, A.W.; Bazmi, A.A.; Zahedi, G.; Klemeš, J.J. A review of progress in renewable energy implementation in the Gulf Cooperation Council countries. *J. Clean. Prod.* **2014**, *71*, 168–180. [CrossRef]
82. Zureikat, Y. *Challenges and Strategies for Increasing Adoption of Renewable Energy in the MENA Region*; Massachusetts Institute of Technology: Cambridge, MA, USA, 2019.
83. Ghaebi, H.; Bahadori, M.N.; Saidi, M.H. Different operational alternatives of aquifer thermal energy storage system for cooling and heating of a residential complex under various climatic conditions in Iran. *Sci. Iran.* **2019**, *26*, 1281–1292. [CrossRef]
84. De Schepper, G.; Paulus, C.; Bolly, P.Y.; Hermans, T.; Lesparre, N.; Robert, T. Assessment of short-term aquifer thermal energy storage for demand-side management perspectives: Experimental and numerical developments. *Appl. Energy* **2019**, *242*, 534–546. [CrossRef]
85. Lu, H.; Tian, P.; Guan, Y.; Yu, S. Integrated suitability, vulnerability and sustainability indicators for assessing the global potential of aquifer thermal energy storage. *Appl. Energy* **2019**, *239*, 747–756. [CrossRef]
86. Gao, L.; Zhao, J.; An, Q.; Liu, X.; Du, Y. Thermal performance of medium-to-high-temperature aquifer thermal energy storage systems. *Appl. Therm. Eng.* **2019**, *146*, 898–909. [CrossRef]
87. Pophillat, W.; Bayer, P.; Teyssier, E.; Blum, P.; Attard, G. Impact of groundwater heat pump systems on subsurface temperature under variable advection, conduction and dispersion. *Geothermics* **2020**, *83*, 101721. [CrossRef]
88. Sathe, S.S.; Mahanta, C. Groundwater flow and arsenic contamination transport modeling for a multi aquifer terrain: Assessment and mitigation strategies. *J. Environ. Manag.* **2019**, *231*, 166–181. [CrossRef]
89. Karimi, L.; Motagh, M.; Entezam, I. Modeling groundwater level fluctuations in Tehran aquifer: Results from a 3D unconfined aquifer model. *Groundw. Sustain. Dev.* **2019**, *8*, 439–449. [CrossRef]
90. Qi, Q.Q.; Xu, Y.X.; Song, S.H.; Zhang, Z.Z. Application of a groundwater modelling system in groundwater environmental impact assessment of river and lake connection in western Jilin region. *Appl. Ecol. Environ. Res.* **2019**, *17*, 5059–5066. [CrossRef]
91. Aquaveo. GMS—Groundwater Modeling System. Available online: <https://www.aquaveo.com/software/gms-groundwater-modeling-system-introduction> (accessed on 5 June 2020).
92. Jaxa-Rozen, M.; Kwakkkel, J.H.; Bloemendal, M. A coupled simulation architecture for agent-based/geohydrological modelling with NetLogo and MODFLOW. *Environ. Model. Softw.* **2019**, *115*, 19–37. [CrossRef]
93. Hameed, M.R.; Kadhim, Y.M.; Abbas, E.H.; Khudhair, Y.S. Simulation of Lowering Groundwater in the Right Bank of Derbendikhan Dam. *Int. J. Civ. Eng. Technol.* **2019**, *10*, 3003–3014.
94. Patil, N.S.; Chetan, N.L.; Nataraja, M.; Suthar, S. Climate change scenarios and its effect on groundwater level in the Hiranyakeshi watershed. *Groundw. Sustain. Dev.* **2020**, *10*, 100323. [CrossRef]
95. Waterloo Hydrogeologic. Visual MODFLOW Flex. Available online: <https://www.waterloohydrogeologic.com/visual-modflow-flex/> (accessed on 5 June 2020).

96. Naranjo-Fernández, N.; Guardiola-Albert, C.; Montero-González, E. Applying 3D geostatistical simulation to improve the groundwater management modelling of sedimentary aquifers: The case of Doñana (Southwest Spain). *Water* **2018**, *11*, 39. [CrossRef]
97. Lekula, M.; Lubczynski, M.W. Use of remote sensing and long-term in-situ time-series data in an integrated hydrological model of the Central Kalahari Basin, Southern Africa. *Hydrogeol. J.* **2019**, *27*, 1541–1562. [CrossRef]
98. Nonterah, C.; Xu, Y.; Osa, S. Groundwater occurrence in the Sakumo wetland catchment, Ghana: Model-setting–scenario approach. *Hydrogeol. J.* **2019**, *27*, 983–996. [CrossRef]
99. United States Geological Survey (USGS). ModelMuse: A Graphical User Interface for Groundwater Models. Available online: <https://www.usgs.gov/software/modelmuse-a-graphical-user-interface-groundwater-models> (accessed on 5 June 2020).
100. Rehman, H.U.; Ahmad, Z.; Ashraf, A.; Ali, S.S. Predicting groundwater potential zones in Upper Thal Doab, Indus Basin through integrated use of RS and GIS techniques and groundwater flow modeling. *Arab. J. Geosci.* **2019**, *12*, 621. [CrossRef]
101. Kaushik, S.; Dhote, P.R.; Thakur, P.K.; Nikam, B.R.; Aggarwal, S.P. An integrated approach for identification of waterlogged areas using RS and GIS technique and groundwater modelling. *Sustain. Water Resour. Manag.* **2019**, *5*, 1887–1901. [CrossRef]
102. Nhu, V.H.; Rahmati, O.; Falah, F.; Shojaei, S.; Al-Ansari, N.; Shahabi, H.; Shirzadi, A.; Górski, K.; Nguyen, H.; Ahmad, B.B. Mapping of groundwater spring potential in karst aquifer system using novel ensemble bivariate and multivariate models. *Water* **2020**, *12*, 985. [CrossRef]
103. Al-Madhloom, Q.; Hamza, B.; Al-Ansari, N.; Laue, J.; Nordell, B.; Hussain, H.M. Site Selection Criteria of UTES Systems in Hot Climate Critères de sélection du site des systèmes UTES dans un climat chaud. In Proceedings of the XVII ECSMGE-2019, Reykjavik, Iceland, 1–7 September 2019.
104. Naicker, K.; Cukrowska, E.; McCarthy, T.S. Acid mine drainage arising from gold mining activity in Johannesburg, South Africa and environs. *Environ. Pollut.* **2003**, *122*, 29–40. [CrossRef]
105. Tomiyama, S.; Igarashi, T.; Tabelin, C.B.; Tangviroon, P.; Li, H. Modeling of the groundwater flow system in excavated areas of an abandoned mine. *J. Contam. Hydrol.* **2020**, *230*, 103617. [CrossRef]
106. Ta, D.; Cao, S.; Steyl, G.; Yang, H.; Li, Y. Prediction of Groundwater Inflow into an Iron Mine: A Case Study of the Thach Khe Iron Mine, Vietnam. *Mine Water Environ.* **2019**, *38*, 310–324. [CrossRef]
107. Bayer-Raich, M.; Credoz, A.; Guimerà, J.; Jordana, S.; Sampietro, D.; Font-Capó, J.; Nief, N.; Grossemy, M. Estimates of Horizontal Groundwater Flow Velocities in Boreholes. *Groundwater* **2019**, *57*, 525–533. [CrossRef] [PubMed]
108. Fang, X.; Xiong, F.; Chen, J. An Experimental Study on Fiber Bragg Grating-Point Heat Source Integration System for Seepage Monitoring. *IEEE Sens. J.* **2019**, *19*, 12346–12352. [CrossRef]
109. Environmental Systems Research Institute ESRI. ArcMap 10.6 (10.6.1) Software. 2018. Available online: <https://support.esri.com/en/products/desktop/arcgis-desktop/arcmap/10-6> (accessed on 5 June 2020).
110. Yacoub, S.Y. Geomorphology of the mesopotamia plain. *Iraqi Bull. Geol. Min.* **2011**, *4*, 7–32.
111. Yacoub, S.Y. Stratigraphy of the Mesopotamia plain. *Iraqi Bull. Geol. Min.* **2011**, *Special Issue*, 47–82. Available online: <https://www.iasj.net/iasj?func=fulltext&aId=61737> (accessed on 9 June 2020).
112. Sissakian, V.K.; Fouad, S.F. Geological map of Iraq, scale 1: 1000 000, 4th edition, 2012. *Iraqi Bull. Geol. Min.* **2015**, *11*, 9–16.
113. Jassim, S.Z.; Goff, J.C. *Geology of Iraq*; Dolin (Prague and Moravian Museum): Brno, Czechia, 2006.
114. Al-Jiburi, H.K.; Al-Basrawi, N.H. Hydrogeology of the Mesopotamia plain. *Iraqi Bull. Geol. Min.* **2011**, *Special Issue*, 1–21.
115. Al-Jiburi, H.K.; Al-Basrawi, N.H. Hydrological map of Iraq, scale 1:1000,000, 2nd edition, 2013. *Iraqi Bull. Geol. Min.* **2015**, *11*, 17–26.
116. Sissakian, V.K.; Buthaina, S.M. Stratigraphy. *Iraqi Bull. Geol. Min.* **2007**, *Special Issue*, 51–124. Available online: <http://ibgm-iq.org/ibgm/index.php/ibgm/article/view/61> (accessed on 3 June 2020).
117. Al-kubaisi, Q.Y.; Al-abadi, A.M.; Al-ghanimy, M.A. Mapping groundwater quality Index for irrigation in the Dibdibba aquifer at Karbala—Najaf plateau, central of Iraq. *Iraqi J. Sci.* **2018**, *59*, 1636–1652.
118. Allaby, M. *A Dictionary of Geology and Earth Sciences*, 4th ed.; Oxford University Press: Oxford, UK, 2013.
119. Hassan, K.M. Stratigraphy of Karbala—Najaf Area, Central Iraq. *Iraqi Bull. Geol. Min.* **2007**, *3*, 53–62.
120. Al-Madhloom, Q.; Al-Ansari, N.; Hussain, H.M.; Lindblom, J.; Abdullah, T.; Hamza, B.A.; Knutsson, S. Seepage Velocity of Dibdibba Formation in Karbala, Iraq. *Engineering* **2017**, *9*, 279–290. [CrossRef]

121. Jassim, R. Gypsum deposits in Iraq: An overview. *Iraqi Bull. Geol. Min.* **2019**, *Special Issue*, 241–261.
122. Gupta, R.S. *Hydrology & Hydraulic Systems*, 4th ed.; Waveland Press Inc.: Long Grove, IL, USA, 2017.
123. Estabragh, A.R.; Soltani, A.; Javadi, A.A. Models for predicting the seepage velocity and seepage force in a fiber reinforced silty soil. *Comput. Geotech.* **2016**, *75*, 174–181. [[CrossRef](#)]
124. Environmental Systems Research Institute (ESRI). ArcMap. Available online: <https://desktop.arcgis.com/en/arcmap/> (accessed on 3 June 2020).
125. Environmental Systems Research Institute (ESRI). Darcy Velocity. Available online: <https://desktop.arcgis.com/en/arcmap/10.3/tools/spatial-analyst-toolbox/darcy-velocity.htm> (accessed on 7 June 2020).
126. Environmental Systems Research Institute (ESRI). How Darcy Flow and Darcy Velocity Work. Available online: <https://desktop.arcgis.com/en/arcmap/10.3/tools/spatial-analyst-toolbox/how-darcy-flow-and-darcy-velocity-work.htm> (accessed on 5 June 2020).
127. Environmental Systems Research Institute (ESRI). Projection Basics the GIS Professional Needs to Know. Available online: <http://webhelp.esri.com/arcgisdesktop/9.3/index.cfm?TopicName=Projectionbasics-the-GIS-professional-needs-to-know#:~:text=Coordinates%20systems%20known%20as,area%20on%20the%20earth%20T1%20text%20quoteright%20surface> (accessed on 7 June 2020).
128. Environmental Systems Research Institute (ESRI). Universal Transverse Mercator (UTM). Available online: http://webhelp.esri.com/arcgisdesktop/9.3/index.cfm?TopicName=Universal_Transverse_Mercator (accessed on 7 June 2020).
129. Al-Ani, A.A. Selection of Best Technique to Evaluate Groundwater Recharge a Case Study of Dibdiba Aquifer in Area of Karbala-Najaf. Ph.D. Thesis, University of Baghdad, Baghdad, Iraq, 2004.
130. Al-Jiburi, H.K.; and Al-Basrawi, N.H. Hydrogeology. *Iraqi Bull. Geol. Min.* **2007**, *Special Issue*, 125–144.
131. Hameed, W. Kriging of Groundwater Level—A Case Study of Dibdiba Aquifer in Area of Karbala-Najaf. *J. Kerbala Univ.* **2008**, *6*, 170–182.
132. Al-Dabbas, M.; Khafaji, R.; Al-Jaberi, M.H. Impact of climate changes on the hydrogeological aquifers- case study Dibdiba aquifer at Karbala Najaf area, Iraq. *Int. J. Res. Sci. Technol.* **2015**, *5*, 24–39.
133. Thabit, J.M.; Khalid, F.H. Resistivity imaging survey to delineate subsurface seepage of hydrocarbon contaminated water at Karbala Governorate, Iraq. *Environ. Earth Sci.* **2016**, *75*, 1–7. [[CrossRef](#)]
134. Al-Sudani, H.I. Hydrogeological Properties of Groundwater in Karbala'a Governorate—Iraq Introduction. *J. Univ. Babylon Eng. Sci.* **2018**, *26*, 70–84.
135. Al-Abadi, A.M.; Handhal, A.M.; Al-Ginamy, M.A. Evaluating the Dibdiba Aquifer Productivity at the Karbala–Najaf Plateau (Central Iraq) Using GIS-Based Tree Machine Learning Algorithms. *Nat. Resour. Res.* **2020**, *29*, 1989–2009. [[CrossRef](#)]
136. Al-Areedhi, H.H. Modelling of Groundwater Flow for the Iraqi Aquifers. Ph.D. Thesis, University of Technology, Baghdad, Iraq, 2019.
137. Saleh, S.A.; Al-ansari, N.; Abdullah, T. Groundwater Hydrology in Iraq. *J. Earth Sci. Geotech. Eng.* **2020**, *10*, 155–197.
138. Al-Ansari, N.; Sissakian, V.K.; Adamo, N. Hydrogeology of the Mesopotamian Plain: A Critical Review. *J. Earth Sci. Geotech. Eng.* **2020**, *10*, 111–124.
139. Al Maimuri, N.M. Radon (222Rn) occurrence in quaternary deposits, annual dosage, and groundwater recirculation in Hashimiya, Iraq. *Sustain. Water Resour. Manag.* **2017**, *5050*, 11. [[CrossRef](#)]

